Author Manuscript

Sensitivity of wintertime Arctic black carbon to removal processes and regional Alaskan sources

Eleftherios Ioannidis[1,2*], Kathy S. Law[2], Jean-Christophe Raut[2], Louis Marelle[2], Tatsuo Onishi[2], Elisabeth Andrews[3,4], Sho Ohata[5], Tatsuhiro Mori[6], Sara Morris[4], Yukata Kondo[7], Sangeeta Sharma[8], Konstantinos Eleftheriadis[9], Zbigniew Klimont[10], Antonin Soulie[11], Claire Granier[3,11,12], Patricia K. Quinn[13], Kerri A. Pratt[14]

[1]Department of Earth Sciences, Vrije Universiteit Amsterdam, Amsterdam, the Netherlands
[2]Sorbonne Université, UVSQ, CNRS, LATMOS, Paris, France
[3]CIRES, University of Colorado and NOAA Chemical Sciences Laboratory, Boulder, CO, USA
[4]NOAA/Global Monitoring Laboratory, Boulder, CO, USA
[5]Institute for Space–Earth Environmental Research, Nagoya University, Nagoya, Aichi, Japan
[6]Department of Applied Chemistry, Faculty of Science and Technology, Keio University, Kanagawa, Japan
[7]National Institute of Polar Research, Tokyo, Japan
[8]Environment and Climate Change Canada, Science and Technology Branch, Toronto, Canada
[9]NCSR "Demokritos"-Institute of Nuclear and Radiological Sciences and Technology, Energy and Safety Environmental Radioactivity Laboratory, Athens, Greece
[10]International Institute for Applied Systems Analysis, Laxenburg, Austria
[11]Laboratoire d'Aérologie, Université de Toulouse, CNRS, UPS, Toulouse, France
[12]NOAA/Chemical Sciences Laboratory, Boulder, CO, USA
[13]Pacific Marine Environmental Laboratory, National Oceanic and Atmospheric Administration, Seattle, Washington, United States
[14]Department of Chemistry and Department of Earth and Environmental Sciences, University of Michigan, Ann Arbor, Michigan, USA

Key Points:

- WRF-Chem captures observed wintertime surface black carbon variability in the Arctic, with results sensitive to removal processes.
- Wet removal influences black carbon at Arctic sites downwind of storm tracks. Sites near Arctic sources are more sensitive to dry removal.
- Regional Alaskan sources, notably from the North Slope Alaskan oil-fields, contribute up to 30% - 50% to black carbon at Utqiaġvik/Barrow.

*Previously at: Sorbonne Université, UVSQ, CNRS, LATMOS, Paris, France

Corresponding author: Ioannidis Eleftherios, e.ioannidis@vu.nl,elefth.ioannidis@gmail.com

This is the author manuscript accepted for publication and has undergone full peer review but has not been through the copyediting, typesetting, pagination and proofreading process, which may lead to differences between this version and the Version of Record. Please cite this article as doi: 10.1029/2024JD042885.

This article is protected by copyright. All rights reserved.

Author Manuscript

Abstract

Air pollutants are primarily transported from mid-latitude emission regions in winter and early spring, leading to elevated concentrations of aerosols, including black carbon (BC), in the Arctic, a phenomenon known as Arctic Haze. The Weather Research and Forecasting model coupled with chemistry is used to investigate potential causes of uncertainties in modeling Arctic BC for winter 2014. The model captures observed variability in BC at surface sites, reproducing BC concentrations at Zeppelin but showing a low bias at Tiksi, Alert, and Utqiaġvik/Barrow. The influence of removal processes on model biases is explored by switching off dry or wet deposition. Wet deposition, during transport in the North Atlantic storm track, and locally over Svalbard, dominates BC removal at Zeppelin, while wet removal in the Pacific storm track influences BC at Alert and Utqiaġvik/Barrow. Dry removal over Asian source regions and Alaska affects BC at Utqiaġvik/Barrow, and is larger than wet removal at Tiksi due to the proximity of local/regional anthropogenic sources. Regional runs over northern Alaska in late January show improved simulated BC compared to observations at Utqiaġvik/Barrow due, in part, to better resolution of removal processes, and local/regional emissions. Sensitivity runs also show that regional Alaskan sources, notably from the North Slope Alaskan oil-fields, may be contributing 30% to 50%, on average, to observed BC at Utqiaġvik/Barrow in January and February 2014, with the remainder from outside the region. These findings highlight the importance of local Arctic emissions, and the need for improved emission inventories in the Arctic.

Plain Language Summary

Black carbon (BC), emitted by incomplete combustion of biomass or fossil fuels, is a short-lived climate forcer contributing to global and Arctic climate warming. BC and other aerosols are transported from emission regions in mid-latitudes into the Arctic during winter and spring, a phenomenon called Arctic Haze. However, there are local sources of BC within the Arctic, such as wood burning for residential heating, gas flaring during oil and gas extraction or power generation, contributing to BC concentrations in the Arctic. In this work, a detailed meteorological and chemical transport model is used to simulate Arctic BC during wintertime. In particular, the influence of processes removing BC from the atmosphere (precipitation, dry deposition) is examined. The model sensitivity to these processes varies across the Arctic, and explains some of the differences with observed BC at Arctic sites. Runs over northern Alaska show an important contribution from local and regional emissions to observed BC, notably from North Slope of Alaska petroleum extraction emissions. The findings from this study highlight the need for improved anthropogenic emissions over the Arctic, as well as important sensitivities to modeled removal processes.

1 Introduction

Black carbon (BC) is a short-lived climate forcer (SLCF) that scatters and absorbs incoming solar radiation, affects aerosol-cloud interactions and, when deposited on snow or ice, can accelerate sea-ice or snow melting. It has been shown to make a significant contribution to rapid warming in the Arctic *(Quinn et al., 2008; Flanner, 2013; Yun et al., 2013; IPCC, 2021; von Salzen et al., 2022)*. Improving the quantification of BC climate effects in the Arctic requires better understanding about BC sources, transport, and removal processes in different seasons, notably in winter, a season that has received less attention. During winter and the winter-spring transition, higher concentrations of aerosols, including BC, are observed in the Arctic, a phenomenon called Arctic Haze *(Rahn & McCaffrey, 1980; Barrie et al., 1994; Quinn et al., 2002)*. This is due to the build up of anthropogenic pollutants transported from mid-latitude emission regions and local, within, or near Arctic sources, coupled with weaker removal processes, and stable atmo-

This article is protected by copyright. All rights reserved.

Author Manuscript

spheric conditions during winter in the Arctic *(Barrie et al., 1981; Quinn et al., 2002; Stohl, 2006)*. Studies have shown that Russian gas flaring, together with residential and industrial combustion, that are higher in very cold Arctic winters, are making important contributions to Arctic BC concentrations *(Winiger et al., 2017, 2019; Zhu et al., 2020; Matsui et al., 2022; Popovicheva et al., 2022)*. For example, *Leaitch et al. (2018a)* estimated that 28% of wintertime BC at Alert in northern Canada may originate from gas flaring emissions in northern Russia and Eurasia. Enhanced wintertime BC at Utqiaġvik/Barrow in northern Alaska has been attributed to mid-latitude fossil fuel combustion sources, together with Russian anthropogenic emissions *(Barrett et al., 2015)*. However, possible contributions from petroleum extraction emissions on the North Slope of Alaska (NSA), also identified as a source of aerosols during winter *(Kolesar et al., 2017; Barrett et al., 2015; Kirpes et al., 2018)*, were not considered.

BC source apportionment studies often rely on model estimates. However, models tend to underestimate Arctic BC during wintertime regardless of the model or emission inventory *(Eckhardt et al., 2015; Shen et al., 2017; Chen et al., 2020; Mori et al., 2020; M. Liu & Matsui, 2021; Whaley et al., 2022)*. These discrepancies could be due to underestimation of mid-latitude or local Arctic emissions *(Stohl et al., 2013; Winiger et al., 2017)*, difficulties simulating transport of pollutants to the Arctic, for example, linked to model resolution *(Ma et al., 2013)*. Another major source of uncertainty in models is related to the simulation of BC wet and dry removal *(Sharma et al., 2013; Mahmood et al., 2016; Shen et al., 2017; Raut et al., 2017; Xu et al., 2019)* affecting BC ageing and lifetimes *(J. Liu et al., 2011; Ikeda et al., 2017; M. Liu & Matsui, 2021)*. Wet and dry BC deposition occur mainly over mid-latitude source regions and during transport to the Arctic, and to a lesser extent within the Arctic. However, during winter, the relative contributions of wet and dry deposition in the Arctic show considerable variability, based on rather limited modeling studies. They tend to show wet removal dominating over dry deposition *(Bourgeois & Bey, 2011; Mahmood et al., 2016)* although *Sharma et al. (2013)* found that dry deposition accounted for 70% of total deposition north of 70°N. In a recent multi-model evaluation, total wet plus dry BC deposition in Greenland and the European Arctic was overestimated compared to limited observations, and may explain why current models still underestimate wintertime Arctic BC *(Whaley et al., 2022)*.

The main goal of this study is to investigate processes influencing simulated wintertime BC in the Weather Research and Forecasting, coupled with chemistry (WRF-Chem) model over the Arctic. There is a particular focus on removal processes and sources over central/northern Alaska. Model simulations are carried out for winter 2014 coinciding with a measurement campaign in Utqiaġvik/Barrow, on the north coast of Alaska. During the campaign observed BC was found to always be internally mixed with organic and sulfate (SO_4^{2-}) aerosols, indicating an anthropogenic influence from background Arctic haze, or more locally from the NSA oil fields to the east *(Kirpes et al., 2018)*. Here, we build on a first study motivated by this campaign, which improved sea-spray aerosols (SSA) emissions in WRF-Chem over the wider Arctic and northern Alaska during winter 2014 *(Ioannidis et al., 2023)*. Results confirmed a possible influence of the NSA oil field emissions on observed non sea-salt (nss)-SO_4^{2-} at Utqiaġvik/Barrow, but their influence on BC over northern Alaska was not investigated. Here, modeled BC is first evaluated against surface observations over the wider Arctic. Then, in order to better understand model discrepancies, the sensitivity of modeled BC to wet and dry deposition within and outside the Arctic is examined. Finally, the sensitivity of modeled BC over northern Alaska to planetary boundary layer (PBL) meteorology, removal processes and local/regional sources, notably the NSA oil-fields, is explored.

The WRF-Chem model, emission inventories, and model simulations are described in Section 2. The BC observations used to evaluate the model are introduced in Section 3. The results are presented in Sections 4, 5 and 6. In Section 4, modeled BC distribu-

This article is protected by copyright. All rights reserved.

Author Manuscript

tions are presented and evaluated at remote Arctic sites. The influence of dry and wet removal on Arctic BC is examined further in Section 5. The results from a regional study focusing on Utqiaġvik/Barrow are presented in Section 6, including the results of model sensitivities. The implications of our findings and conclusions are provided in Section 7.

2 Methodology

2.1 WRF-Chem model setup

The WRF-Chem model version 3.9.1.1 is used to perform quasi-hemispheric and regional simulations to investigate Arctic BC. WRF-Chem is a fully coupled, online meteorological and chemical transport mesoscale model *(Grell et al., 2005)*. In this study, a modified version by *Marelle et al. (2017)* and *Ioannidis et al. (2023)* is used. The model setup, including meteorological and chemical parametrizations, is the same as in *Ioannidis et al. (2023)*. Briefly, the Yonsei University (YSU) boundary layer, Mesoscale Model Version 5 similarity (MM5) surface layer, and NOAH Multi-parameterization (MP) Land Surface Model are used. The model is run with Gas-phase chemistry & Statewide Air Pollution Research Center (SAPRC-99, *Carter (2000); Marelle et al. (2017)*) and the Model for Simulating Aerosol Interactions and Chemistry (MOSAIC) aerosol scheme *(Zaveri et al., 2008)*. MOSAIC includes processes affecting aerosols in the atmosphere, such as nucleation, evaporation, coagulation, condensation, deposition and aerosol-cloud interactions. The size distribution of each aerosol species is represented by eight bins between 39 nm and 10 μm. All the particles in a bin are assumed to be internally mixed, and both mass and number are predicted. As a result, aerosols are aged when emitted (coagulated with other species). MOSAIC includes grid scale *(Morrison, 2009)* and subgrid scale *(Berg et al., 2015)* aqueous chemistry. Dry deposition accounts for aerodynamic resistance, surface layer resistance, and Brownian diffusion, to estimate dry deposition velocities of aerosols, including BC, based on the *Binkowski and Shankar (1995)* parameterisation, following *Slinn and Slinn (1980)* and *Slinn (1982)*. Aerosol sedimentation in MOSAIC is calculated throughout the atmospheric column, based on the Stokes velocity scheme, as described in *Marelle et al. (2017)*. Wet removal of aerosols by grid-resolved stratiform clouds (precipitation) includes in-cloud and below-cloud removal by rain, snow, and graupel by Brownian diffusion, interception, and impaction mechanisms following *Easter et al. (2004)* and *Chapman et al. (2009)*. In-cloud wet removal occurs when cloud droplets including aerosols are converted to precipitation. Wet removal of aerosols and trace gases is included in the cumulus cloud parameterisation scheme *(Berg et al., 2015)*. Removal due to subgrid-scale convective clouds is also included in MOSAIC, as described in previous studies *(Marelle et al., 2017; Raut et al., 2017)*. Wet and dry deposition are calculated for each size bin, with total deposition over all bins as model output. This MOSAIC version has improved treatment of wintertime SSA emissions including a sea-surface temperature dependence, higher wind speed dependence in the Arctic, and sources of sea-salt SO_4^{2-} and marine organics, as described in *Ioannidis et al. (2023)*.

2.2 Model simulations

Two simulation domains (polar stereo-graphic projection) are used in this study, as shown in Figure 1. The first (parent) domain (d01) covers a large part of the Northern Hemisphere with 100 km horizontal resolution. Boundary and initial conditions are derived from National Centers for Environmental Prediction Final meteorological reanalysis data (NCEP FNL 1°x1°) *(National Centers for Environmental Prediction, National Weather Service, NOAA, U.S. Department of Commerce, 2000)* and Model for OZone And Related chemical Tracers (MOZART) *(Emmons et al., 2010)* for atmospheric trace gases and aerosols. The nested domain (d02), run at a horizontal resolution of 20 km, covers continental Alaska, a small area of northwest Canada, and the Chukchi and Beau-

This article is protected by copyright. All rights reserved.

Author Manuscript

fort Seas (Figure 1.). Grid nudging is used for the 100 km resolution domain, while spectral nudging is applied at 20 km, and spectral nudging parameters are calculated as in *Hodnebrog et al. (2019)*. 50 pressure levels are used in both domains. WRF-Chem temperatures and winds are nudged to the reanalysis, at each dynamical step above the PBL, and are updated every 6 hours.

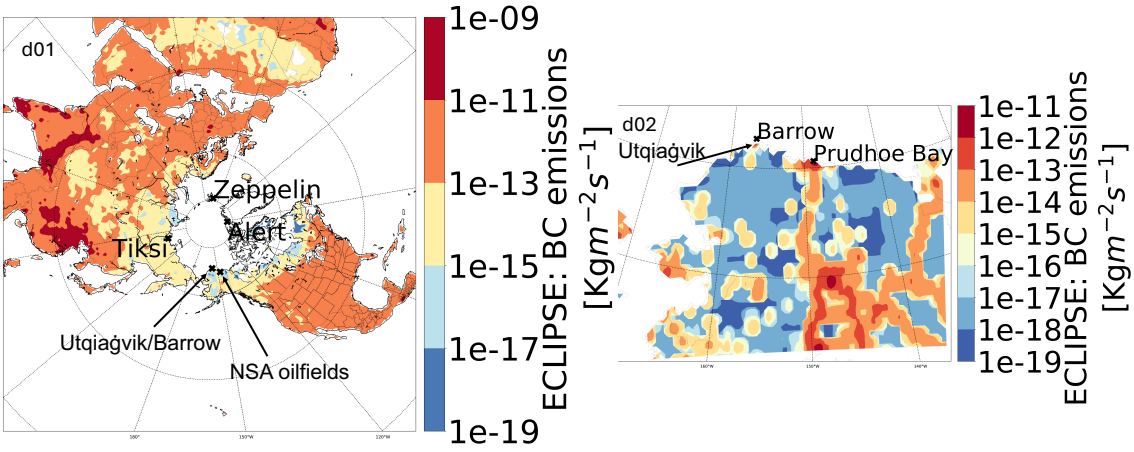


Figure 1. Average BC emissions (ECLIPSE v6b), in kg m^{-2}s^{-1}, for January and February 2014, interpolated on a WRF-Chem domain at 100 km (d01: left map), and January 2014 at 20km (d02: right map). The map on the left shows the locations of four Arctic observation sites used in this study, and the location of the North Alaskan Oil-fields (NSA). The map on the right shows the location of Prudhoe Bay within the NSA oil-fields, the Barrow Observatory and village of Utqiaġvik. Note the different scales for the BC emissions.

The model is run at 100 km from November 2013 to February 2014 with the first two months considered as spin up. The model is run at 20 km over central and northern Alaska from 23 to 28 January 2014 and 24 to 28 February 2014 corresponding to the Utqiaġvik field campaigns *(Kirpes et al., 2018, 2019)*, as in *Ioannidis et al. (2023)*. For the regional simulations, 4 days prior to the beginning of each campaign are treated as spin up. All model results are output every 3h. The simulations, including the base CONTROL run and sensitivity runs are summarized in Table 1, and discussed in the following sections. To evaluate model performance compared to observed BC at Arctic sites, different statistical parameters are calculated (see Table A.1, APPENDIX 1).

2.3 Emissions

2.3.1 Anthropogenic emissions

ECLIPSE inventory

Anthropogenic emissions from the Evaluating the Climate and Air Quality Impacts of Short-Lived Pollutants version 6 (ECLIPSE v6b) inventory, with a resolution of 50 km are used in the simulations at quasi-hemispheric and regional scale for winter 2013–2014 *(Amann et al., 2011; Klimont et al., 2017; Höglund-Isaksson et al., 2020; Whaley et al., 2022)*. Nine sectors are included in the ECLIPSE v6b inventory: agriculture (livestock), residential, energy, industry, gas flaring and venting, international shipping, transportation, waste, and solvent use. Figure 1 shows BC average emissions at 100 km during January and February 2014, and at 20 km over northern Alaska during January 2014.

This article is protected by copyright. All rights reserved.

Author Manuscript

Table 1. Description of WRF-Chem model simulations. See text for details.

Simulation Name	Description
Quasi- hemispheric simulations (100 km)	
CONTROL	Base simulation
WET_DEP_OFF	Wet deposition OFF
DRY_DEP_OFF	Dry deposition OFF
Regional simulations over Alaska (20 km)	
ALASKA_CONTROL	Base simulation
DRY_DEP_OFF_20km	Dry deposition OFF
WET_DEP_OFF_20km	Wet deposition OFF
METEO	Mellor-Yamada-Janjic (MYJ) boundary layer scheme
ANTHR_OFF	Alaskan anthropogenic emissions OFF
CAMS_ANTHR	CAMS anthropogenic emissions over Alaska
ANTHR_5x	5x Alaskan anthropogenic emissions (ECLIPSE v6b)

CAMS inventory

Anthropogenic emissions from Copernicus Atmosphere Monitoring Service (CAMS) are implemented in the January 2014 run over northern Alaska in a sensitivity simulation (Section 6.3). CAMS emissions are based on Community Emissions Data System version 2 (CEDSv2, *McDuffie et al. (2020)*) and Emissions Database for Global Atmospheric Research version 5 (EDGAR v5) inventories *(Crippa et al., 2019)*. CAMS version 5.3 emissions are available at 10 km resolution *(Soulie et al., 2023)*, a higher spatial resolution than ECLIPSE v6b. Eight sectors are included: agriculture (livestock and soils), power plants, fugitives, industry, oil refineries and transformation industry, residential and commercial combustion, shipping, solid waste and waste water, road and off-road transportation. For all simulations, the anthropogenic emissions (ECLIPSE and CAMS) are only emitted at the surface in this study.

2.3.2 Natural emissions

Emissions of Dimethyl Sulphide (DMS), mineral dust, and lightning NO_x are calculated online (*Marelle et al. (2017)* and references within). Biogenic emissions for 2014 are calculated online from Model of Emissions of Gases and Aerosol from Nature (MEGAN) inventory *(Guenther et al., 2012)*. SSA emissions are based on *Ioannidis et al. (2023)*.

3 Black carbon observations

Observations collected at four surface sites in the Arctic are used to evaluate model BC during January and February 2014 using a variety of different filter-based absorption photometry measurement techniques depending on location (see Table 2). Three of the four sites (Alert, Tiksi, Zeppelin) utilized an aethalometer (Magee AE-31) to measure aerosol absorption coefficients (b_{abs}). At Utqiaġvik/Barrow, both a Particle Soot Absorption Photometer (Radiance Research PSAP) and continuous soot monitoring sys-

This article is protected by copyright. All rights reserved.

Author Manuscript

tem (COSMOS) were used to obtain b_{abs}. We first describe the different instruments, and then the sites, and specific data treatments, where applicable.

Table 2. Black carbon surface observations at Arctic sites. Latitudes and longitudes are given for the sites, together with mean altitude above sea-level (masl) in m. TSP stands for Total Suspended Particles. NA stands for Not Applicable. See text for details and definitions.

Metrics/Sites	Alert (Canada) 82.5N, -63.3W 185 masl	Utqiaġvik/Barrow (USA) 1.3N, -156.6W 11 masl	Tiksi (Russia) 71.6N, 128.9E 8 masl	Zeppelin (Norway) 78.9N, 11.9W 475 masl
Instruments	AE-31	PSAP, COSMOS	AE-31	AE-31
MAC (m^2/g)	16.6	13.5, NA	16.6	15.9
Size cutoff (μm)	TSP	1, 1	10	1
Wavelength (nm)	880	660, 565	880	880
Wind sector screening	no	yes, no	yes	no
Time averaging	24h	hourly, hourly	hourly	24h
Data source	Environment Canada	NOAA,Space-Earth Research Japan	NOAA	EBAS

3.1 Filter-based absorption photometers

All sites used filter-based absorption photometers to derive Elemental Black Carbon (EBC). Here, EBC observations with diameters smaller than 1.0 μm ($d_p \leq 1.0$ μm) are defined as sub-micron. In the case of $d_p \leq 10$ μm then EBC is defined as total EBC, and used to compare with Total Suspended Particles (TSP) observations. The model results are shown for the same size cut-offs as the observations, as discussed in *Ioannidis et al. (2023)*. All observations are in UTC. More information about each instrument is provided below.

Aethalometer: AE-31 aethalometers measure the attenuation of light transmitted through particles accumulating on a quartz fiber filter at seven wavelengths (370, 470, 520, 590, 660, 880, and 950 nm). Aerosol absorption coefficient data in 1/mega-meters [Mm^{-1}], observed using aethalometers, is obtained for Zeppelin and Alert from the European Monitoring and Evaluation Programme (EMEP) via EBAS and Enviroment Canada, respectively, and for Tiksi from National Oceanic and Atmospheric Administration (NOAA). A multiple scattering constant, C_{ref}, equal to 3.5, consistent with the findings of *Backman et al. (2017)*, is applied to account for aethalometer scattering artifacts for all three sites. EBC values are calculated from aethalometer aerosol absorption coefficients at 880 nm to minimize potential interference from other absorbing components (e.g. brown carbon) *(Sharma et al., 2017, 2019)*. *Backman et al. (2017)* estimated 36% relative uncertainty for this instrument, due to particle loading and scattering that cannot be determined. For each site a constant mass absorption coefficient (MAC), in m^2g^{-1}, is applied to the b_{abs} data to give EBC mass concentrations in ngm^{-3} (Table 2). MAC relates the optical attenuation through the filter to BC mass concentrations. More information about the AE-31 Aethalometer can be found in different studies (e.g. *Sharma et al. (2017)*, *Backman et al. (2017)*, *Ohata et al. (2020)*).

This article is protected by copyright. All rights reserved.

Author Manuscript

COSMOS: Measurements using a COSMOS instrument at Utqiaġvik/Barrow are used in this study. This instrument has been developed to measure the mass concentrations of BC *(Miyazaki et al., 2008; Kondo et al., 2009, 2011; Ohata et al., 2020)*. COSMOS derives light absorption coefficients at 565 nm from the change in transmission through a quartz-fiber filter after loading with BC particles *(Kondo et al., 2009; Ohata et al., 2019)*. Further information about how COSMOS estimates BC is given in *Ohata et al. (2020)*. *Ohata et al. (2019)* estimated the accuracy of COSMOS BC measurements to be 10% compared to BC measured with single-particle soot photometers at different sites.

PSAP: Like the aethalometer and COSMOS, PSAP obtains b_{abs} based on the change in transmission through a filter as particles accumulate on the filter *(Bond et al., 1999; Ogren, 2010)*. The PSAP measures transmission at three wavelengths (467, 530 and 660 nm). Here, PSAP data measured at Utqiaġvik/Barrow at wavelength 660 nm (red) are used. Measurement uncertainties in PSAP data depend on uncertainties in the flow meter calibration (1.5 %), and measurement of spot size (2 %) *(Sharma et al., 2017)*. PSAP b_{abs} is corrected for instrument non-idealities using the *Bond et al. (1999)* correction with the *Ogren (2010)* adjustment for multiple wavelengths.

3.2 Arctic observatories

Zeppelin: This station is located near to Ny-Alesund, on Svalbard. Daily b_{abs} at 880 nm wavelength from an AE-31 are used to estimate sub-micron EBC, by applying a MAC of 15.9 m^2g^{-1} at 880 nm. Local pollution events, such as from cruise ship visits to Ny-Alesund, are removed. More information is provided in *Eleftheriadis et al. (2009)*.

Tiksi: This site is located in northern Siberia, on the coast of the Laptev Sea and is surrounded by tundra. To determine total EBC, hourly b_{abs} from an AE-31 at 880 nm is used with a MAC value of 16.6 m^2g^{-1} *(Asmi et al., 2016)*. Data are reported every 5 minutes, but hourly averages are used to compare to model results. The Tiksi Observatory (referred to as Tiksi from now on) is located south of the Tiksi urban settlement. Wind direction and wind speed criteria are applied to sampling at this site to remove local pollution from Tiksi. More specifically, data are removed when wind directions are between 315° and 45°, and wind speeds are less than 1 ms^{-1} *(Asmi et al., 2016)*.

Alert: The observatory is located on the edge of the Lincoln Sea at the northeastern tip of Ellesmere Island, Nunavut, northern Canada. A MAC equal to 16.6 m^2g^{-1} is used to estimate daily fine mode EBC from AE-31 measurements *(Sharma et al., 2017)*. *Backman et al. (2017)* reported an uncertainty of 2.5% at Alert when accounting for noise only, and a 1.5% uncertainty in flow rate, as reported by the manufacturer. Local interference from the nearby military base camp is removed from the data.

Utqiaġvik/Barrow: The NOAA Barrow Atmospheric Baseline Observatory is located near the village of Utqiaġvik on the north coast of Alaska (referred to as Utqiaġvik/Barrow). Hourly PSAP and COSMOS data are used here to compare to the model results. To calculate EBC from the PSAP data, a MAC is calculated following *Ohata et al. (2020)*. MAC equal to 13.5 m^2g^{-1} is derived based on the slope of the relationship between b_{abs} and COSMOS-BC for sub-micron particles. During January and February 2014, b_{abs}-PSAP and COSMOS-BC are highly correlated (r^2 = 0.92, not shown here). COSMOS is operated with a sub-micron size cutoff, while the PSAP is downstream of a switched impactor system which switches between a 1.0 μm and 10 μm size cutoff every 30 min. Here, only sub-micron PSAP data are used. COSMOS data includes all wind sectors, while PSAP data excludes air masses originating from the wind sector 130° to 360°, and when wind speeds are less than 0.5 ms^{-1}, to exclude local Utqiaġvik village pollution influences *(Quinn et al., 2002)*.

This article is protected by copyright. All rights reserved.

Author Manuscript

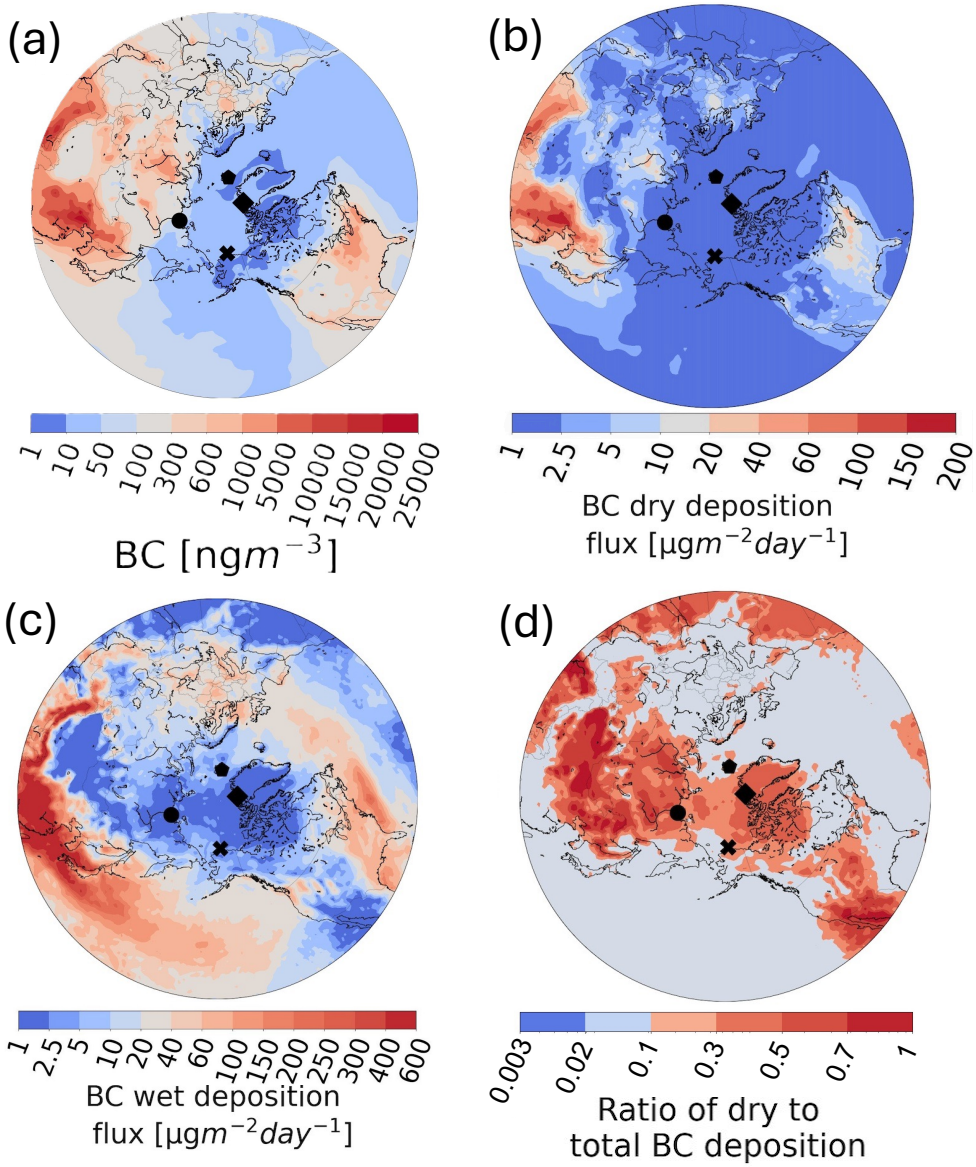


Figure 2. (a) Surface modeled BC concentrations in ng m^{-3}, and (b) dry deposition fluxes, (c) wet deposition fluxes in μg m^{-2} day^{-1}, and (d) the ratio of dry deposition flux to total dry plus wet deposition fluxes (unit-less) at the surface. Results are averages over January and February 2014 from the CONTROL run. The different symbols show the location of the four sites. Circle: Tiksi, X: Utqiaġvik/Barrow, diamond: Alert, and pentagon: Zeppelin.

4 Evaluation of modeled Arctic wintertime BC

Here, modeled BC distributions, and wet and dry deposition fluxes, over the Arctic and mid-latitude source regions are discussed, and simulated BC concentrations are evaluated against surface observations over the wider Arctic. Results are shown from the CONTROL run with ECLIPSE v6b anthropogenic emissions. Model results include the full size range, except for the evaluation against surface data when size ranges corresponding to the measurements are used.

Figure 2a shows average modeled surface BC during January and February 2014 over the hemispheric domain from CONTROL. The highest modeled concentrations are

This article is protected by copyright. All rights reserved.

Author Manuscript

found over source regions in China and India, reaching up to 25,000 ng m^{-3} with lower concentrations, of the order of 100-1000 ng m^{-3}, simulated over Europe and North America. The WRF-Chem results are in broad agreement with previous studies, such as *Luo et al. (2020)* and *Backman et al. (2021)*, who reported simulated BC of 200-600 ng m^{-3} over North America and Europe during winter. Modeled BC concentrations are an order of magnitude lower over the Arctic, and generally below 50 ng m^{-3}, except over Siberia where BC reaches up to 5000 ng m^{-3} due to Russian anthropogenic emissions.

Figure 2 also shows average surface dry (Fig. 2b) and wet (Fig. 2c) BC deposition fluxes as well as the ratio of dry BC deposition fluxes to total dry plus wet BC deposition fluxes at the surface (Fig. 2d). The highest deposition fluxes are simulated over mid-latitude source regions, in particular over Asia, with average dry deposition fluxes, of up to 200 μg m^{-2} day^{-1} and wet deposition fluxes up to 600 μg m^{-2} day^{-1}, respectively. While simulated wet deposition fluxes are higher than those reported by *Matsui et al. (2022)* over Asia (250 μg m^{-2} day^{-1}) using the Community Atmosphere Model with the Aerosol Two-dimensional bin module for foRmation and Aging Simulation (CAM-ATRAS) model, total modeled BC deposition fluxes during winter are generally of similar magnitudes compared to other modeling estimates *(Jiao et al., 2014; Moffett et al., 2022)*. On average, WRF-Chem wet deposition fluxes are up to 3 times higher than dry deposition fluxes at the surface, as illustrated in Fig. 2. *Mahmood et al. (2016)* also found that wet deposition exceeded dry deposition during winter over mid-latitude source regions in 3 out of 4 of participating models in that study. However, as shown in Fig. 2, dry deposition can also exceed wet deposition at the surface, depending on location.

In the Arctic, WRF-Chem wet deposition fluxes tend to be higher than dry deposition fluxes, in particular over areas influenced by the northerly extension of the Pacific and North Atlantic storm tracks. For example, over Alaska, and the Barents Sea and the area around Svalbard, wet deposition fluxes range from 5–20 μg m^{-2} day^{-1}. Dry deposition fluxes are low in the Arctic, except over Russian source regions where they reach 40 μg m^{-2} day^{-1} (see Fig. 2b). Total wet plus dry fluxes (1–2 μg m^{-2} day^{-1}) are similar over the Arctic Ocean, and higher, by up to 5-10 times, than those diagnosed in an Aerosol Comparisons between Observations and Models (AEROCOM) multi-model evaluation *(Jiao et al., 2014)* (depending on the model). Overall, WRF-Chem wet and dry BC deposition fluxes are lower in the Arctic, in agreement with *Mahmood et al. (2016)*. Regional and altitude differences in Arctic wet and dry deposition, together with evaluation against available observed fluxes, are discussed in the next section.

Table 3. Statistical evaluation of modeled BC from the CONTROL run against observed BC at four Arctic sites for January and February 2014. All statistics are calculated using daily (24h mean) average modeled and observed values. See text for details. See Table A1 for definitions.

Statistical metrics/Sites	Alert	Utqiaġvik/Barrow (COSMOS/PSAP)	Tiksi	Zeppelin
Median model (ng m^{-3})	11.0	12/14	67	11
Median observations (ng m^{-3})	35	30/25	187	10
RMSE (ng m^{-3})	44	29/22	193	16
Bias (ng m^{-3})	-28	-20/-16	-150	-4
NME (%)	68%	62%/55%	68%	59%
NMB (%)	-65%	-60%/-53%	-66%	-32%

This article is protected by copyright. All rights reserved.

Author Manuscript

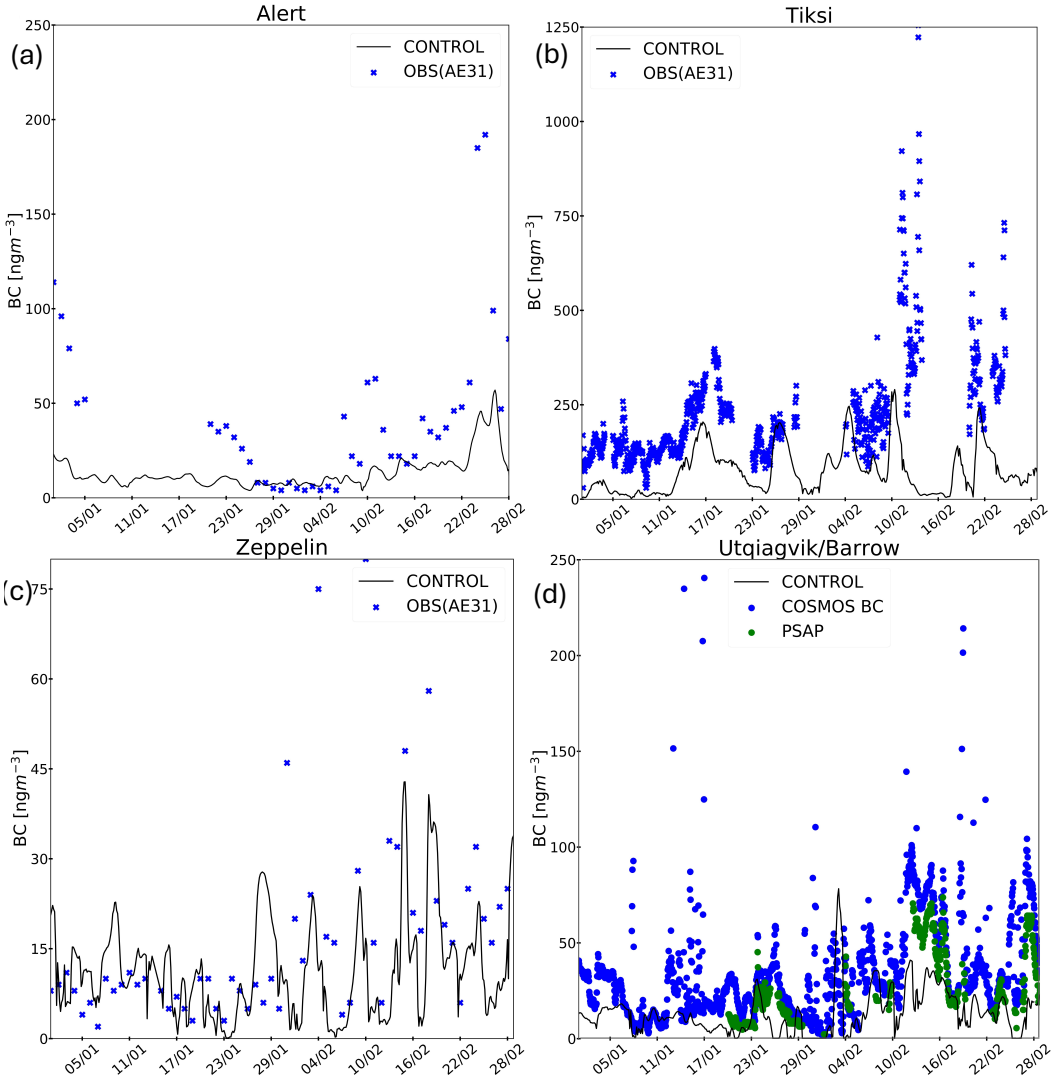


Figure 3. Modeled BC compared to available surface observations, in ng m^{-3}, of (a) daily TSP EBC at Alert, (b) hourly total EBC at Tiksi, (c) daily sub-micron EBC at Zeppelin, and (d) hourly sub-micron EBC at Utqiaġvik/Barrow, Alaska during January and February 2014. All times are UTC. The black line shows model results from the CONTROL run. EBC observations, including sub-micron COSMOS data at Utqiaġvik/Barrow, are shown as blue crosses. Green diamonds show sub-micron PSAP EBC at Utqiaġvik/Barrow. Model results are 3-hourly and for same size ranges as the observations. Note the different scales.

Model results from the CONTROL run are also compared to observed EBC at four Arctic sites (Tiksi, Zeppelin, Alert and Utqiaġvik/Barrow) during January and February 2014 in Figure 3. Table 3 displays the statistical evaluation of the model results compared to the observations, together with median observed and modeled concentrations for the different sites (all 24 hour (daily) averages).

The highest EBC is observed at Tiksi with a median EBC concentration of 187 ng m^{-3}. This site is situated on the north coast of Russia and influenced by Eurasian anthropogenic emissions, as shown in Figure 2. The model simulates higher concentrations at Tiksi with a model median BC that is up to five times higher than at other Arctic sites during winter 2014, but underestimates the observations by about a factor of 3 (nor-

This article is protected by copyright. All rights reserved.

Author Manuscript

malized mean biases (NMB) of -66%). This is largely because, while the model captures observed temporal variability, it underestimates episodes with higher observed concentrations (500-1250 ng m^{-3}). Tiksi measurements may be influenced by local emissions, such as trash burning, power generation, and transport (*Popovicheva et al. 2019*), even though a local contamination (wind direction) filter has been applied.

Observed EBC at Utqiaġvik/Barrow varies between 1–250 ng m^{-3} with higher concentrations measured by the COSMOS instrument which samples all wind directions, whereas PSAP EBC does not show the same elevated concentrations since local influences are removed. The model captures observed variability at this site, even if it underestimates observed COSMOS EBC by around 20 ng m^{-3} on average (NMB of -60%). Observed episodes with higher BC (up to 220 ng m^{-3}) are underestimated, and simulated BC does not exceed 80 ng m^{-3}. The model compares better to the PSAP observations (which exclude local pollution), with lower bias and RMSE, than compared to COSMOS data.

Periods with higher concentrations are also observed at Alert, in particular at the end of February when observed daily EBC reaches up to 200 ng m^{-3} on a couple of days. The model is also biased low at this site (bias of -28 ng m^{-3}, NMB -65%), but simulates higher concentrations towards the end of February, up to 55 ng m^{-3}. High concentrations in the observations are attributed to long-range transport from remote sources, since any influence from the nearby military camp is removed, and there are no other local emission influences at Alert *(Leaitch et al., 2018b)*.

The lowest wintertime EBC is observed at Zeppelin. The model reproduces the observed range of EBC at Zeppelin (5–75 ng m^{-3}), as well as observed increases in February. There is good agreement between the observed (10 ng m^{-3}) and model (11 ng m^{-3}) medians leading to low model bias at this site (-4 ng m^{-3}, NMB -32%).

Overall, the model captures observed temporal and spatial variability between these sites but underestimates concentrations, notably during episodes with enhanced EBC, during winter 2014. It reproduces increases in BC in February compared to January 2014. Modeled negative biases in this study are in agreement with the AMAP multi-model evaluation, including WRF-Chem, even when updated emissions are used in both studies including, for example, increases in Russian gas flaring in ECLIPSE v6b *(Whaley et al., 2022)*. The influence of removal processes, and local/regional sources over Alaska, on modeled BC, that may be contributing to model biases, are examined in the following sections.

5 Sensitivity of simulated BC to wet and dry removal

To examine the effect of removal processes on Arctic BC during wintertime, sensitivity simulations are performed with wet and dry deposition switched off (see Table 1). Results are presented over the hemispheric domain including mid-latitude source regions and the Arctic, as well as at the sites discussed in the previous section. In the sensitivity runs, either wet deposition in grid-scale clouds and parameterized cumulus clouds (WET_DEP_OFF) or dry deposition, including gravitational settling throughout the atmospheric column, are switched off (DRY_DEP_OFF). Figures 4 and 5 show absolute differences in modeled BC between these sensitivity runs and CONTROL at the surface, 2, 4 and 8 km.

When wet removal is turned off modeled surface BC increases by up to 2000 ng m^{-3} on average over Asia and India (Figure 4). Wet removal also affects BC up to 8 km altitude downwind of mid-latitude emission regions. Over the Arctic, the largest surface increases are found over continental regions, such as northwestern Russia (up to 150 ng m^{-3}), with lower effects over the central Arctic Ocean (up to 60 ng m^{-3}). Wet deposition influences modeled BC over northern Alaska due to the northerly extension of the

This article is protected by copyright. All rights reserved.

Author Manuscript

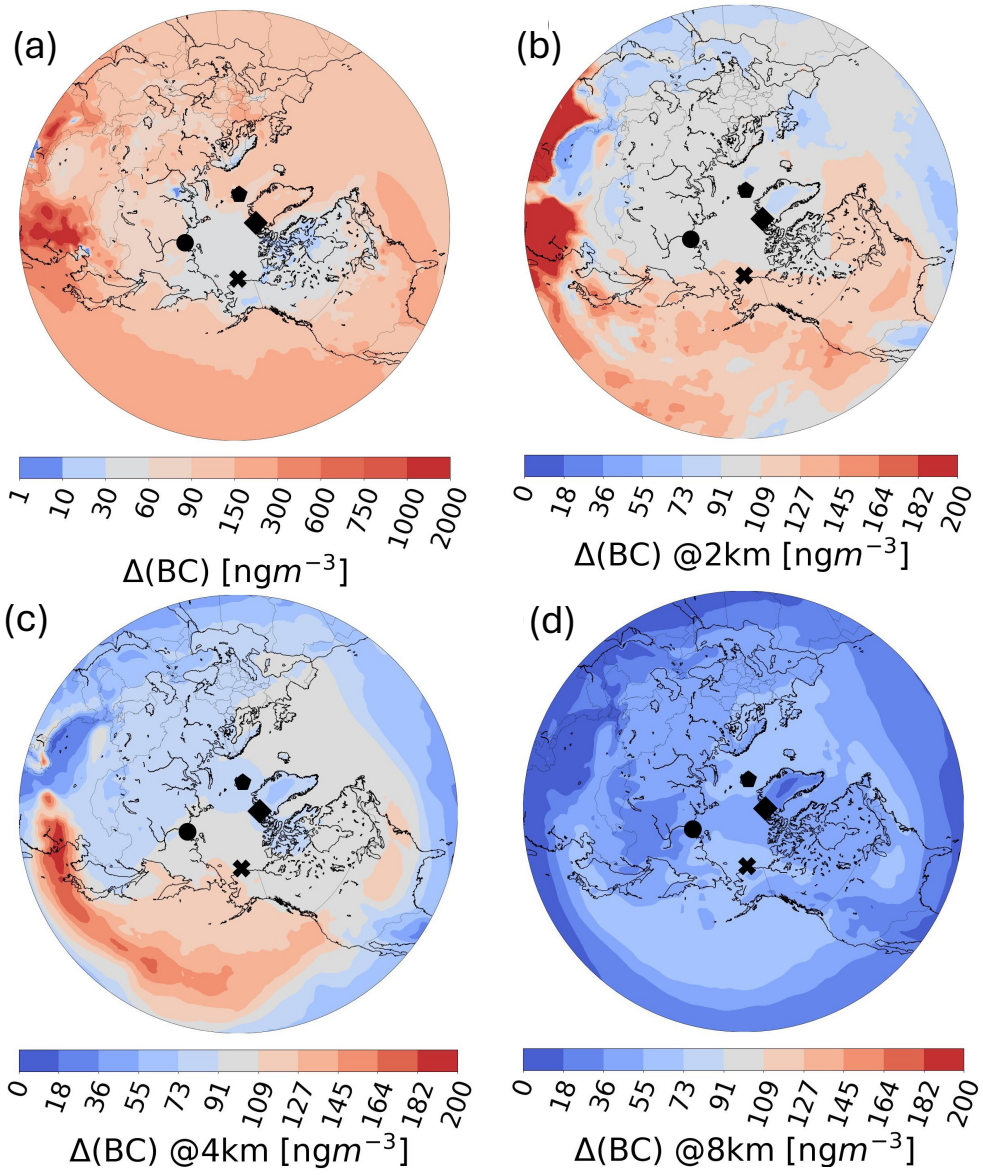


Figure 4. Absolute differences in modeled total BC in ng m^{-3} between WET_DEP_OFF and CONTROL at (a) the surface, (b) 2 km, (c) 4 km, (d) 8 km averaged over January and February 2014.

Pacific storm track up to 8 km, with changes of up to 145 ng m^{-3} at 2-4 km. Wet deposition also affects BC over the Barents Sea, and around Svalbard, as a result of effective pollution transport into the Arctic by air masses originating from Europe and northern Russia during wintertime and the winter-spring transition *(Stohl, 2006; AMAP, 2015)*. Effects are mainly limited to below 2km although some influence from frontal uplift (clouds) linked to the North Atlantic storm track is also evident in BC differences at 4 km.

Similar increases in modeled surface BC are found over continental mid-latitude emission regions (up to 2000 ng m^{-3}) when dry deposition is switched off (Figure 5). Larger increases, than when wet deposition is switched off, are found over Siberia where Russian emissions are located (up to 300 ng m^{-3}). The influence of dry deposition is also seen at the surface over the Arctic Ocean (up to 60 ng m^{-3}), and northern Alaska (up to 30 ng m^{-3}), due to upwind emissions over Russian and Alaska. BC also increases above the

This article is protected by copyright. All rights reserved.

Author Manuscript

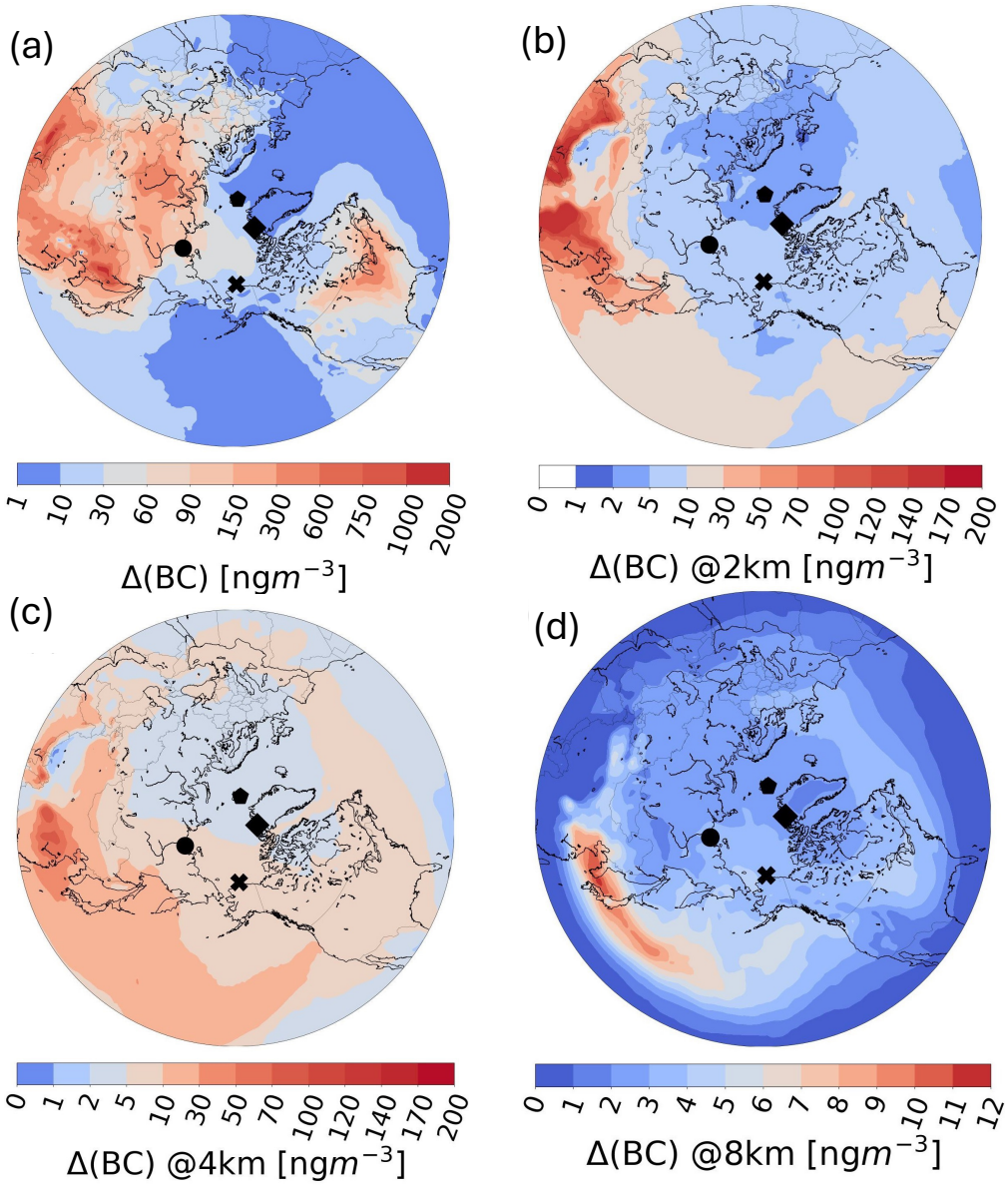


Figure 5. Absolute differences in modeled total BC in ng m^{-3} between DRY_DEP_OFF and CONTROL at (a) the surface, (b) 2 km, (c) 4 km and (d) 8 km averaged over January and February 2014.

surface when dry deposition is switched off since more BC is transported above the PBL and then downwind, albeit to a lesser extent as altitude increases, compared to the wet deposition sensitivity results. Increases vary from 200 ng m^{-3} at 2 km to 70 ng m^{-3} at 4 km, over source regions, notably China, with smaller impacts aloft (up to 12 ng m^{-3} at 8 km).

Figure 6 shows the effect of switching off wet or dry deposition over the hemispheric domain on modeled surface BC concentrations at the four Arctic sites during January and February 2014. In each case, this includes the effects of BC deposition over mid-latitude emission regions, during transport into the Arctic, and deposition of BC from Arctic emissions. Note that switching off one deposition process can also lead to compensating changes in the other removal process. Table 4 shows average relative and absolute changes in sur-

This article is protected by copyright. All rights reserved.

Author Manuscript

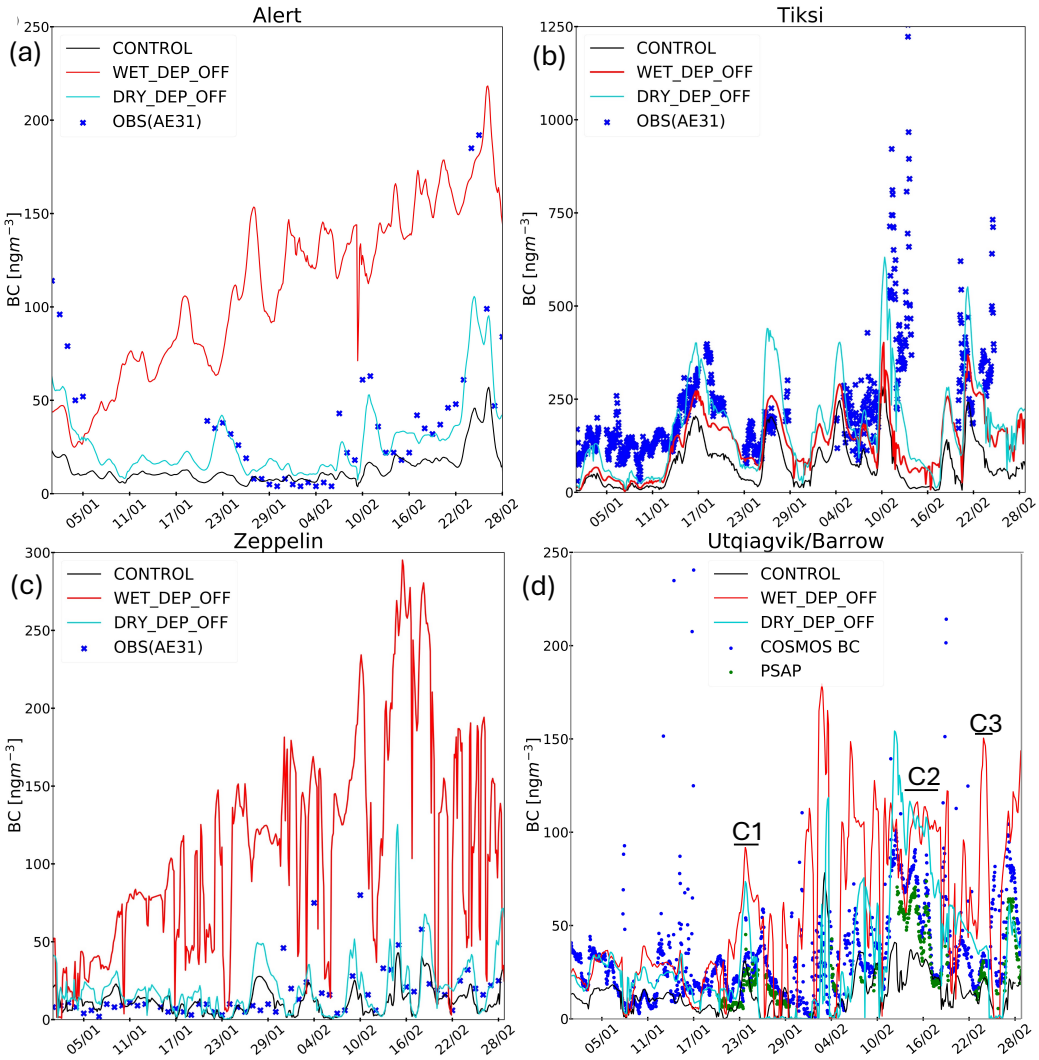


Figure 6. Time series of observed (a) daily TSP EBC at Alert, (b) hourly total EBC at Tiksi, (c) daily sub-micron EBC at Zeppelin, and (d) hourly sub-micron EBC at Utqiaġvik/Barrow, in ng m^{-3} in UTC during January and February 2014. Black line shows model results (3-hourly) from CONTROL, the red line shows WET_DEP_OFF run, and dark turquoise line shows DRY_DEP_OFF run. Alert, Zeppelin, Tiksi: EBC observations are shown in blue crosses. Utqiaġvik/Barrow: EBC observations are shown in blue crosses (COSMOS) and green triangles (PSAP) in UTC. Note that the scales are the same only for Alert and Utqiaġvik/Barrow. See text for details including discussion about particular episodes (C1, C2, C3) indicated on the Utqiaġvik/Barrow time series.

face BC due to wet and dry deposition over this period at the measurement sites. The results show the sensitivity of modeled BC to both processes, and provide indications about their contribution to variability in modeled BC, and potentially in the observations.

At Alert and Zeppelin, average increases in modeled BC in the run with no wet deposition are large, up to +96 and +97 ng m^{-3} respectively, compared to the other two sites (Table 4). Wet deposition occurs during transport of air masses by low-level or during frontal transport pathways (e.g. see *AMAP (2015)*), with an increasing influence of

This article is protected by copyright. All rights reserved.

Author Manuscript

Table 4. Average relative (%) and absolute (ng m^{-3}) changes in modeled BC due to switching off wet or dry deposition at four Arctic sites during January and February 2014 at the surface. Relative changes are calculated as $\frac{(deposition-off_run-CONTROL)}{CONTROL}$ multiplied by 100%.

	Wet Deposition		Dry Deposition	
	% change	Absolute change	% change	Absolute change
Alert	722 %	96	110 %	15
Utqiaġvik/Barrow	317 %	42	151 %	20
Tiksi	78 %	58	137 %	102
Zeppelin	844 %	97	93 %	9

wet removal from January to February at both sites. This may be due to the break-down of the polar dome at the end of winter *(Stohl, 2006)*, and transport of more humid air masses, associated with more precipitation in the Arctic in the late winter/early spring *(Macdonald et al., 2017)*. In contrast to others sites, where local precipitation peaks in summer, Zeppelin, located on Svalbard, experiences maximum precipitation during winter-spring. This suggests that local wet deposition, as well as deposition during transport, influences BC at this site *(Freud et al., 2017; Heslin-Rees et al., 2024)*, whereas it appears that BC at Alert, situated further north, is influenced by wet deposition during transport to the Arctic. *Zieger et al. (2023)* showed that cloud scavenging of BC in January and February (averaged from 2015 to 2019) at Zeppelin is close to zero (0.1 - 0.2). The scavenged fraction is calculated using our model results at Zeppelin, when surface clouds are present and excluding cloud free periods, giving a ratio equal to 0.13, that is close to the range reported by *Zieger et al. (2023)*. This provides some confidence in the performance of the model wet deposition scheme and the parametrization of the aerosol microphysical properties, even if the study years are different. Changes when dry deposition is switched off are smaller at both sites, but appear to correlate with observed EBC. This may suggest a more local or regional influence of dry deposition on BC at these sites.

At Utqiaġvik/Barrow, modeled BC is sensitive to both wet and dry removal but, on average, exhibits a higher sensitivity to wet deposition, with increases of 42 ng m^{-3} compared to 20 ng m^{-3}, respectively (see Table 4). Examples of episodes when removal processes may explain low modeled BC compared to the observations are indicated in Figure 6d. For example, between 23 and 24 January (event 1, C1, Fig. 6) modeled BC from the run with no dry deposition has a narrower peak that corresponds better with the observations. This suggests that issues related to modeled dry deposition are contributing to underestimates in CONTROL BC. On the other hand, low modeled BC between 10 and 16 February (event 2, C2, Fig. 6) could be due to both wet and dry removal, and due to wet removal between 23 and 24 February (event 3, C3, Fig. 6). Model discrepancies between 23-28 January are examined in more detail in the next section.

In contrast to the other sites, modeled BC at Tiksi is more sensitive to dry than wet removal, with average BC increases of 102 and 58 ng m^{-3}, respectively, in the runs with wet and dry removal off. There are sporadic episodes when wet deposition may also be contributing to low modeled BC at Tiksi, such as on 22 February 2014. Overall, these results show that modeled BC at these Arctic sites is more sensitive to wet deposition at Zeppelin and Alert, to dry deposition at Tiksi, and to both removal processes at Utqiaġvik/Barrow.

To investigate this further, modeled BC deposition fluxes are also examined at the different sites (Figure B1), and compared qualitatively to, albeit very limited, observed fluxes. Modeled fluxes are local to each site and provide insights into the role of local-scale removal processes. Modeled BC wet deposition fluxes are similar in magnitude (episod-

This article is protected by copyright. All rights reserved.

Author Manuscript

ically up to 6–8 μg m^{-2} day^{-1}) at Zeppelin, Utqiaġvik/Barrow, and Tiksi. Average fluxes are at the low end of the range of wintertime wet deposition fluxes reported by *Mori et al. (2021)* (2–9 μg m^{-2} day^{-1}) at Ny Alesund in Svalbard, but higher than *Jacobi et al. (2019)* who reported similar contributions from wet and dry deposition of the order of 1–1.5 μg m^{-2} day^{-1}, at this site. Modeled BC wet deposition fluxes at Utqiaġvik/Barrow are episodic, and slightly higher, on average, than reported observed wintertime fluxes of 1–3 μg m^{-2} day^{-1} *(Mori et al., 2020; Matsui et al., 2022)*. Modeled dry deposition fluxes are similar to wet deposition fluxes, in terms of magnitudes and ranges, but less sporadic, at all sites except Alert. At Alert modeled dry deposition fluxes are higher (1–2 μg m^{-2} day^{-1}) than wintertime fluxes reported by *Macdonald et al. (2017)* of around 0.4 μg m^{-2} day^{-1} and modeled wet deposition is very episodic (up to 3.0 μg m^{-2} day^{-1}).

The results presented here provide insights into the influence of removal processes on modeled BC in the Arctic showing that there are significant spatial variations in wet and dry deposition patterns during winter. In addition to removal over mid-latitude source regions, wet deposition has an important influence on surface Arctic BC over Svalbard/Barents Sea and over the northern Pacific/Alaska. On the other hand, dry deposition is more important over northern Russia, and both processes contribute over the Arctic Ocean. This is in contrast to *Sharma et al. (2013)* who found that dry deposition dominated BC removal north of 70N in winter, but in agreement with other studies *(Mahmood et al., 2016; Moffett et al., 2022)*. Simulated wet and dry deposition fluxes are similar to previous estimates over mid-latitude source regions. In the Arctic, lower BC observed at Zeppelin is reproduced by the model, and is due to efficient removal of BC by wet deposition during low-level transport in winter and spring. These results support the observation-based findings of *Freud et al. (2017)* and *Gilardoni et al. (2023)* although local modeled wet deposition fluxes at Zeppelin may be somewhat low compared to more recent flux measurements *(Mori et al., 2021)*. Modeled BC at Alert is also very sensitive to wet removal suggesting that excessive wet deposition during transport in the model is contributing to low model biases at this site. Modeled BC at Utqiaġvik/Barrow is sensitive to both wet and dry removal, and local modeled wet deposition fluxes are somewhat higher than observed estimates *(Mori et al., 2020)*. On the other hand, model sensitivity to dry deposition often correlates with variability in the BC observations at all Arctic sites, and in particular at Tiksi where model BC is influenced more by dry than wet deposition. However, local modeled dry deposition fluxes may be too high, based on comparison with very limited data at Alert *(Macdonald et al., 2017)*. Deficiencies in the treatments of dry deposition or PBL meteorology could explain low modeled surface BC in winter.

This analysis focuses on winter 2014. Wet deposition may vary from year to year depending, in part, on precipitation amounts and trends. *Moon et al. (2024)* showed that winter 2014 is within +/- 10% of the 1991-2020 average and that wintertime precipitation increased in the Arctic over this period. *Heslin-Rees et al. (2024)* also showed that precipitation has been increasing at Zeppelin, contributing to long-term reductions of light-absorbing aerosols from 2002 to 2023. Dry deposition may also vary from year to year depending on transport patterns and PBL stability.

6 Regional BC over northern Alaska

Above, the quasi-hemispheric simulations are used to investigate the influence of removal processes on modeled BC over the wider Arctic. Here, the domain is narrowed, and the sensitivity of modeled BC to regional processes and BC sources over northern Alaska is examined. Here, the results are discussed with respect to *Kirpes et al. (2018, 2019)*. Hence, we refer specifically to the Prudhoe Bay region discussed in these studies, which is within the NSA oil-fields. The model is run at higher resolution (20 km) for the first campaign period described by *Kirpes et al. (2018)* (Section 2.2). The 100 km CONTROL run is used to provide initial and boundary conditions for these shorter runs. The analysis focuses on understanding BC variability at Utqiaġvik/Barrow dur-

This article is protected by copyright. All rights reserved.

Author Manuscript

ing the campaign which took place between 23-28 January 2014. Sensitivities to PBL meteorology, local wet and dry removal, and Alaskan anthropogenic emissions are explored to examine possible reasons for model biases over northern Alaska (see Table 1).

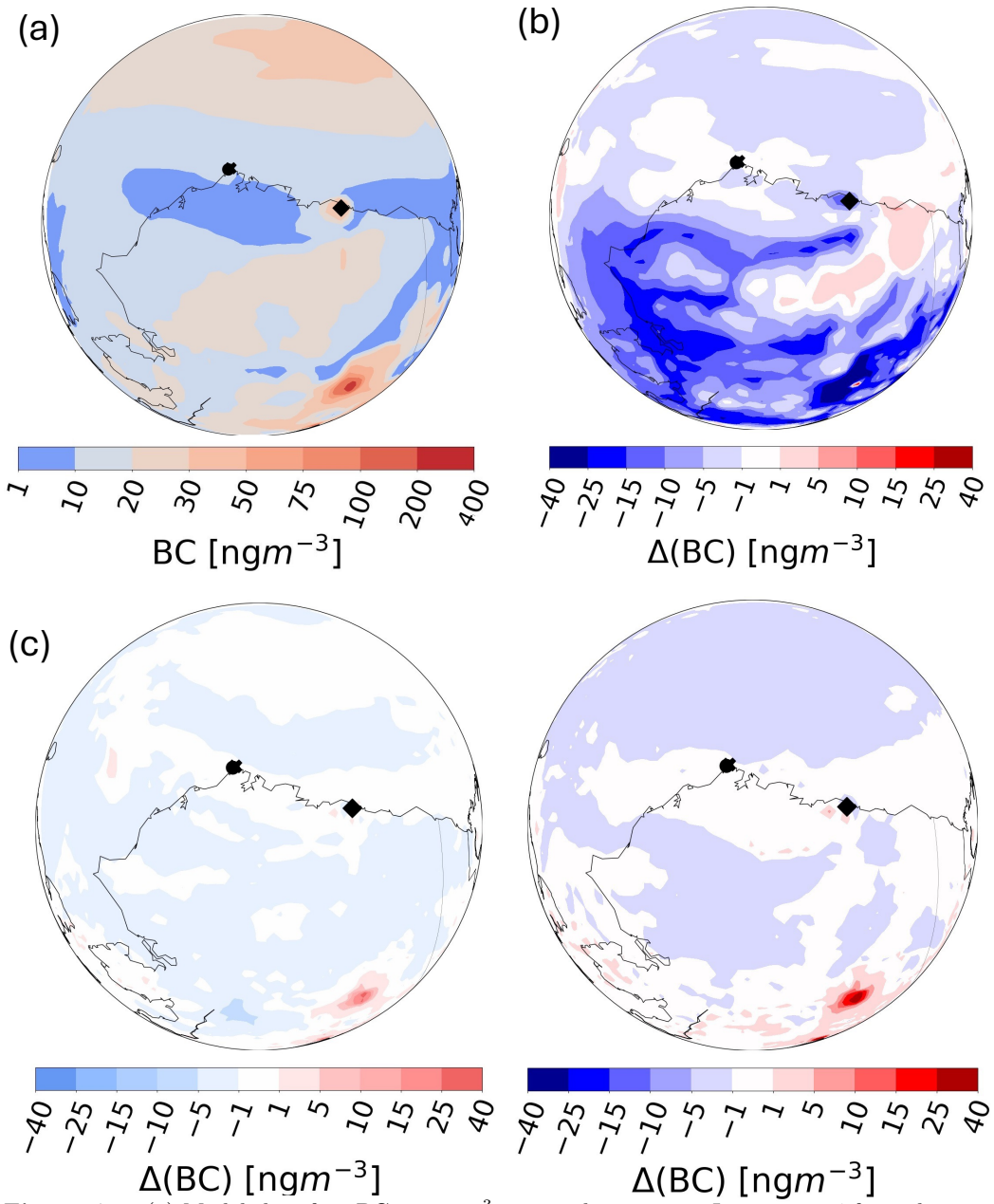


Figure 7. (a) Modeled surface BC in ng m^{-3} averaged over 23-28 January 2014 from the ALASKA_CONTROL run. Average differences in BC concentrations between (b) METEO, (c) WET_DEP_OFF_20km, (d) DRY_DEP_OFF_20km and ALASKA_CONTROL during the January simulation period. The black dot indicates the location of Utqiaġvik/Barrow, while the black diamond indicates the location of Prudhoe Bay in the NSA region.

Figure 7a shows the average BC concentrations for January 2014 at 20 km resolution over northern Alaska from the ALASKA_CONTROL run. The model simulates more BC over central and northern Alaska, by up to 30 ng m^{-3} on average, than in the

This article is protected by copyright. All rights reserved.

Author Manuscript

100 km CONTROL simulation (Fig. 2a). This is due to better resolution of anthropogenic sources at 20 km, in particular over the Fairbanks region in central Alaska and over northern Alaska due to NSA oil-field emissions (up to 75 ng m^{-3} in that region).

Figure 8 shows modeled BC from CONTROL and ALASKA_CONTROL compared to COSMOS-BC and PSAP EBC observations at Utqiaġvik/Barrow during the January 2014 campaign. Observed BC during this campaign varies between 10 and 59 ng m^{-3} with small differences between COSMOS and PSAP measurements (up to 10 ng m^{-3}), in particular during episodes with enhanced BC. Notably, there are no PSAP data when winds were outside the defined clean sector (0–130 degrees), to exclude possible influences from the village of Utqiaġvik situated 8 km south-west of the Barrow Observatory, whereas no wind criteria are applied to the COSMOS measurements. The model captures observed BC reasonably well during the first two days (23-24 January) at 20 km and 100 km. In the earlier analysis of aerosol samples by *Kirpes et al. (2018)*, the 24 January aerosol was mainly dominated by fresh (nascent, non-chloride depleted) SSA, consistent with an Arctic Ocean origin, and also showed an Arctic haze influence (enhanced nss-SO_4^{2-} aerosols) *(Ioannidis et al., 2023)*. On 26 January, *Kirpes et al. (2018)* found more anthropogenic influence in the form of internally mixed BC, organic, and nss-SO_4^{2-} aerosols. However, modeled BC at 100 km is very low (below 5 ng m^{-3}) between 25-26 January. BC is somewhat higher in the 20 km run, except around 00 UTC on 26 January. PSAP EBC data was excluded due to local influences from the village of Utqiaġvik on 26 January, whereas COSMOS measured high EBC up to 59 ng m^{-3} during these 2 days. During the last 2 days of the campaign (27-28 January), PSAP EBC and COSMOS BC do not exceed 20 and 30 ng m^{-3}, respectively. Modeled BC at 20 km agrees reasonably well with the observations while simulated BC at 100 km is too low. *Kirpes et al. (2018)* found higher fractions of individual aerosols containing internally mixed BC, organics, and nss-SO_4^{2-} during this period with air masses originating from the east indicating a stronger NSA oilfield influence.

In general, the model performs slightly better at 20 km than at 100 km with biases and RMSEs decreasing from -16 to -13 and 20 to 16 ng m^{-3}, respectively (Table C2, APPENDIX C), compared to COSMOS BC. Notably, the model performs well on the 27-28 January compared to the CONTROL simulation. Biases and RMSEs are lower compared to PSAP EBC data which excludes pollution from the village of Utqiaġvik. Possible causes contributing to model discrepancies are investigated further in the following sections.

6.1 Boundary layer meteorology

During wintertime Arctic regions are often characterized by stable, shallow PBLs, which trap air pollutants near the surface *(Brümmer & Thiemann, 2002)*. Previous studies have shown that such meteorological conditions play an important role in the formation and transport of atmospheric pollutants during wintertime and the winter-spring transition (e.g. *Tran and Mölders (2011); Bei et al. (2012); Regmi et al. (2019)*). Correct simulation of aerosol removal, in particular dry deposition, also depends on the ability of models to capture PBL structure including vertical profiles of temperature and winds. Results from ALASKA_CONTROL are compared to meteorological data at Utqiaġvik/Barrow (APPENDIX C). Observed temperatures were coldest from 23-25 January (-22 to -18 °C) accompanied by higher wind speeds (10 to 14 m s^{-1}), locally from the east. Winds were calmer (4 to 8 m s^{-1}) from 26-28 January, and from the southeast at the site. The model captures the magnitude and variations in surface temperature, wind speeds and wind directions (Fig. C1). Radiosonde data shows a marked presence of surface temperature inversions below 500 m, together with increasing winds up to this altitude that, along with wind direction, are simulated well by the model. These results suggest that modeled discrepancies in BC are not due to issues simulating the PBL and meteorology around Utqiaġvik/Barrow during the January campaign.

This article is protected by copyright. All rights reserved.

Author Manuscript

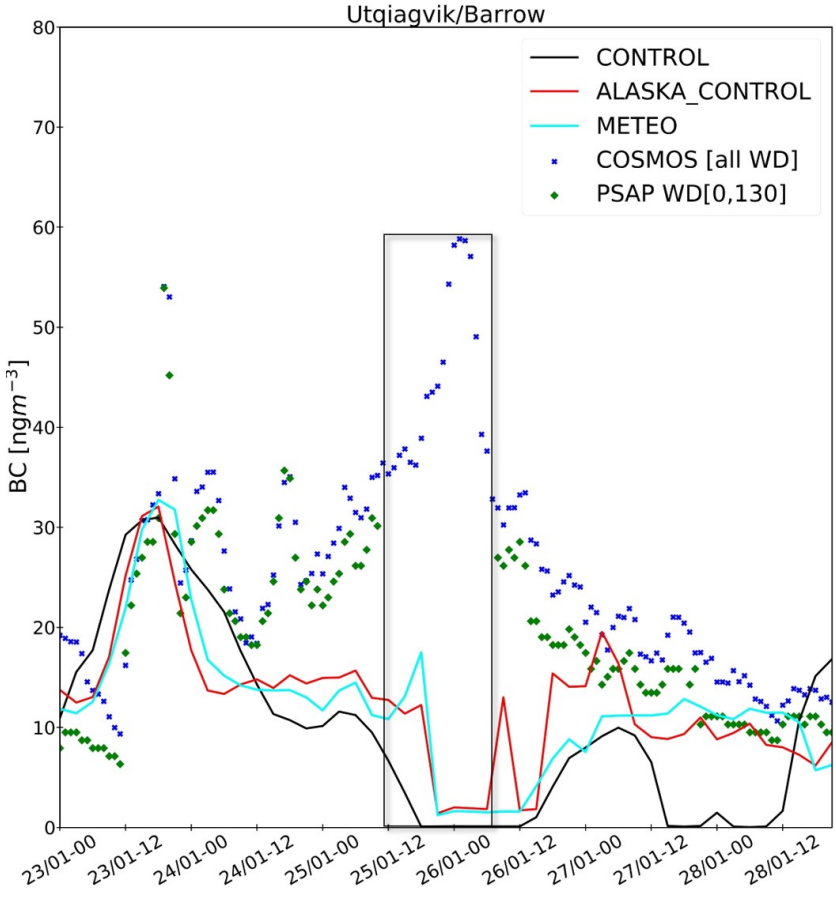


Figure 8. Model evaluation of sub-micron BC, in ng m^{-3}, at Utqiaġvik/Barrow during 23–28 January 2014. Black line shows BC from the CONTROL run at 100 km. Red line shows the ALASKA_CONTROL run at 20 km. Turquoise line shows BC for the sensitivity simulation METEO. Observations are blue crosses (COSMOS) and green diamonds (PSAP). Model results and observations are in UTC. The boxed area shows when there is influence from Utqiaġvik village. All wind directions (WD) for COSMOS data means that observations are not filtered for wind directions, while WD[0,130] for PSAP data excludes these wind directions. See text for details.

To explore PBL influences further, the model is also run with the MYJ (Mellor–Yamada–Janjic) PBL scheme (METEO run), instead of YSU PBL scheme, for the January campaign. Details about the MYJ scheme, and comparison of the runs are provided in APPENDIX C, including statistical evaluation (Table C2). Overall, ALASKA_CONTROL performs better than METEO and CONTROL which tend to be too windy at the surface and show bigger fluctuations at 2 and 10 m temperature, respectively. Figure 7b shows that BC in the run with MYJ has similar BC over the north coast of Alaska. Lower BC to the south over mountainous areas, such as the Brooks Range, and the Fairbanks area, are due to the model simulating more precipitation in METEO (see discussion in APPENDIX C). It can be noted that both simulations underestimate observed precipitation at Utqiaġvik/Barrow (not shown here). However, as shown in Fig. 8, simulated BC at Utqiaġvik/Barrow is similar in both runs, and there are only small differences of up to 0.1 μg m^{-2} day^{-1} in wet and dry deposition fluxes (not shown here). Nevertheless, these results illustrate that modeled BC over northern Alaska is sensitive to PBL treatments, as already discussed in Section 5.

This article is protected by copyright. All rights reserved.

Author Manuscript

6.2 Removal processes

Analysis of the sensitivity runs at 100 km showed that BC during the January campaign at Utqiaġvik/Barrow is influenced by wet deposition on several occasions but had a higher sensitivity to dry deposition on 23-24 January (event C1, Fig. 6d). These simulations include BC deposition over remote and within Arctic source regions, as well as during transport to northern Alaska. Runs switching off wet or dry removal over Alaska are used to examine the sensitivity of modeled BC to local to regional-scale removal processes over the short period at the end of January 2014. Differences between WET_DEP_OFF_20km and ALASKA_CONTROL, show that, when wet deposition is switched off, surface BC is higher over the NSA oil-fields and Fairbanks source regions by up to 5 and 40 ng m^{-3}, respectively (see Fig. 7c). These increases lead to small decreases in surface BC elsewhere. Changes are also small above 2 km (up to 3 ng m^{-3}, not shown). Increases in surface BC due to switching off dry deposition (Fig. 7d) are similar. BC increases by up to 10 ng m^{-3} over the NSA oil fields, and by up to 40 ng m^{-3} over the Fairbanks region in the run without dry deposition.

Modeled wet and dry deposition fluxes of BC at 20 km and 100 km are also compared at Utqiaġvik/Barrow in Fig. 9. Local wet deposition fluxes are lower at 20 km compared to 100 km, and compared to *(Mori et al., 2020)*. Differences are influenced by changes in clouds and PBL structure in the smaller versus the larger domain. In both simulations, there is local BC dry deposition at the site on 23-24 January, followed by wet deposition on 24-25 January. Difficulties capturing observed precipitation are contributing to uncertainties in modeled wet deposition. However, precipitation amounts are underestimated, on average, over the January campaign, at Alaskan sites, including the precipitation (snow) event on 25 January at Utqiaġvik/Barrow (see discussion in APPENDIX C). This simulated wet deposition "event" is of similar magnitude at 100 km and 20 km, albeit with slightly different timing, but fluxes during the dry deposition "event" are much lower at 20 km compared to 100 km. This could be explained by better resolution of the Alaskan emissions, and associated removal near these emissions, at 20 km leading to improved representation of the observed enhancement in BC on 23 January (see Fig. 8). However, this does not explain BC underestimates on 24-25 January, and could be due to issues related to transport of BC to the site or the emissions. The very low modeled BC on 25-26 January, in particular at 100 km, can also not be explained by local wet or dry deposition at the site, but rather processes occurring during transport to northern Alaska. However, on 27-28 January, there is a wet removal episode in the 100 km run that does not occur at 20 km that may explain the very low modeled BC at 100 km (Fig. 8). Differences in the size distribution of BC in air masses transported to northern Alaska, compared to those with local or regional origins, could potentially explain the differences between the large-scale and regional simulations. The extent to which model discrepancies could also be due to Alaskan emissions are discussed in the next section.

6.3 Alaskan emission influence

The sensitivity of modeled BC to regional and local Alaskan anthropogenic emissions is examined over Alaska and at Utqiaġvik/Barrow during the short period of the January campaign. To identify periods when observed BC may be influenced by regional sources, the model is run with Alaskan anthropogenic (ECLIPSE v6b) emissions switched off, and also with regional anthropogenic emissions multiplied by a factor of 5. In a further sensitivity test, the model is run with CAMS instead of ECLIPSE v6b anthropogenic emissions. The only difference between the set-up in the two runs are the anthropogenic emissions.

Surface BC is reduced in the run with Alaskan anthropogenic emissions switched off by 30 to 110 ng m^{-3} over the Prudhoe Bay oil-fields and Fairbanks emission regions, respectively, with smaller reductions of 3-15 ng m^{-3} around Utqiaġvik/Barrow and else-

This article is protected by copyright. All rights reserved.

Author Manuscript

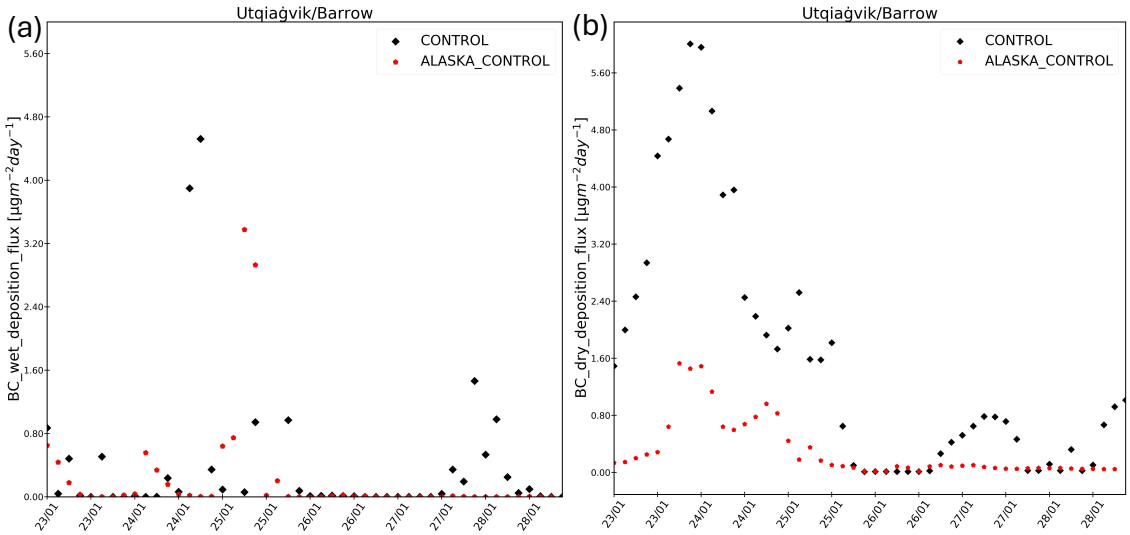


Figure 9. Comparison of modeled (a) wet deposition fluxes, and (b) dry deposition fluxes of BC from runs at 100 km (CONTROL) and 20 km (ALASKA_CONTROL) at Utqiaġvik/Barrow. Wet and dry removal fluxes are in μg m^{-2} day^{-1}.

where over northern Alaska (Fig. 10a). The sensitivity of model results to the NSA oil field emissions is highlighted further in the run with five times more Alaskan anthropogenic emissions (ANTHR_5x) which leads to large increases in BC of up to 300 ng m^{-3} over the Prudhoe Bay area (Fig. 10b). This test also illustrates that there are local BC emissions near the village of Utqiaġvik in the ECLIPSE inventory. The ECLIPSE v6b inventory includes BC emissions from domestic, transportation, industry and energy sectors at Utqiaġvik, but their magnitude is one to three times smaller than the gas flaring emissions from the NSA oil-fields (see Fig. 1).

The use of CAMS emissions leads to lower BC over the Prudhoe Bay oil-fields, by up to 60 ng m^{-3}, and by up to 10 ng m^{-3} west of Utqiaġvik village (Fig. 10c). This is due to lower oil-field emissions in this inventory that includes emissions from oil refineries, industry, energy plants, as well as due to lower transportation and residential emissions in the village of Utqiaġvik and over the Prudhoe Bay oil-fields. In contrast, BC is higher locally, by up to 180 ng m^{-3}, over Fairbanks, but lower in the surrounding area. This is due to a more detailed representation of energy, industry and residential sectors in the CAMS inventory at 10 km resolution compared to the ECLIPSE inventory at 50 km resolution.

Results from these sensitivity runs are compared to observations at Utqiaġvik/Barrow in Fig. 11. Differences between modeled BC in Alaskan ALASKA_CONTROL and ANTHR_OFF suggest that regional Alaskan emissions are influencing BC at this site in January 2014. Based on differences between these runs, Alaskan emissions are estimated to contribute around 30%, on average, to BC during the campaign. Contributions are higher, up to 60%, on 27–28 January when air masses originate from the east and are impacted by the NSA oil-field emissions. The model is also run for the campaign period in the last week of February 2014 (not shown).

The influence of the NSA oil-fields in January is confirmed by the results from ANTHR_5x with large increases in modeled BC on 27–28 January. The results also illustrate a strong sensitivity to Alaskan emissions earlier in the campaign. As noted earlier, observed BC on 25 and 26 January is influenced by local Utqiaġvik emissions when COSMOS BC data shows strong enhancements, and PSAP data shows higher BC before and

This article is protected by copyright. All rights reserved.

Author Manuscript

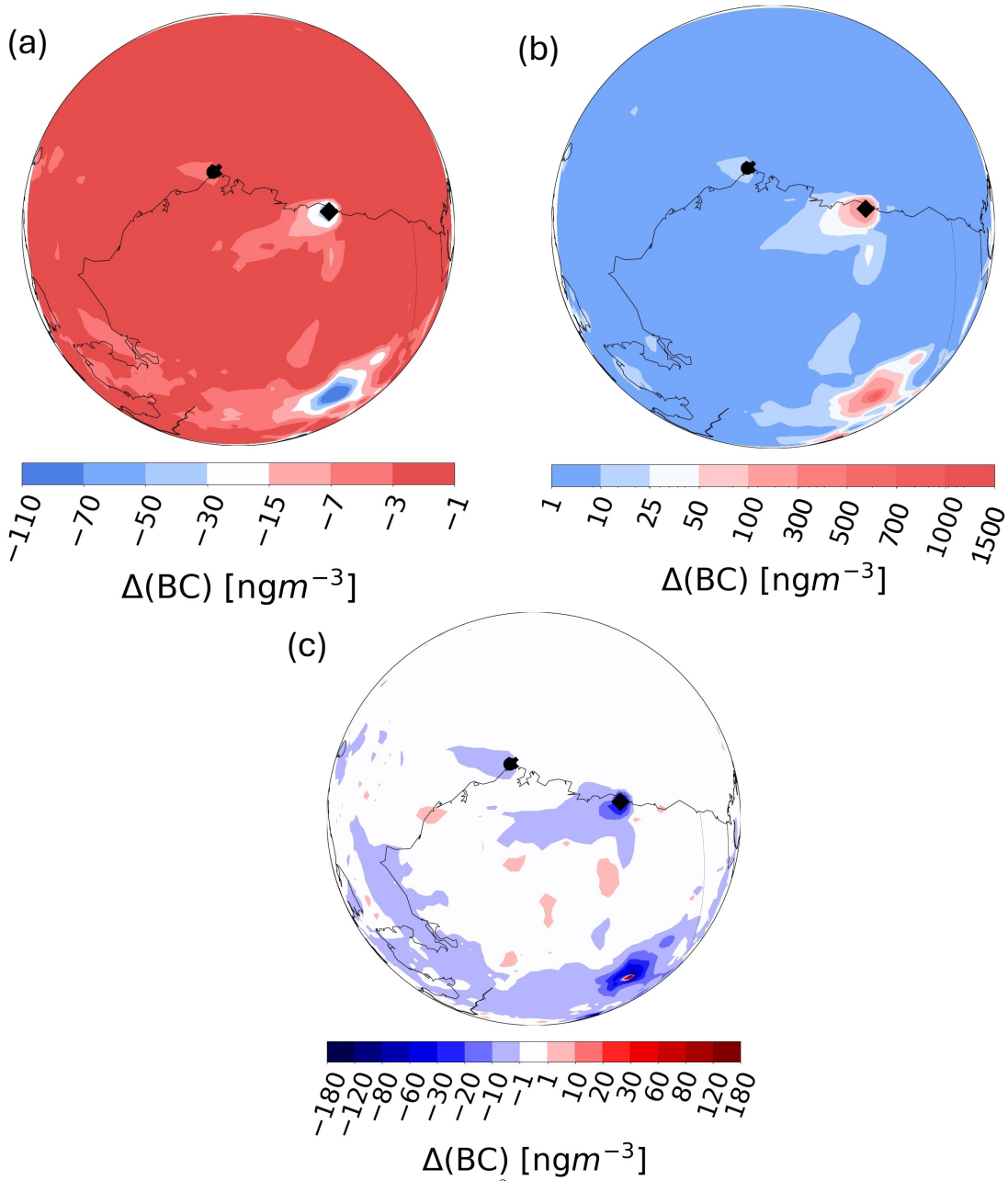


Figure 10. Average differences in BC, in ng m^{-3}, between (a) ANTHR_OFF, (b) ANTHR_5x, (c) CAMS_ANTHR and ALASKA_CONTROL during the January campaign. Black dot indicates the location of Utqiaġvik/Barrow, black "X" indicates the location of Barrow Observatory, and black diamond the location of Prudhoe Bay.

after data is filtered out. The fact that modeled BC increases on 24-25 January in ANTHR_5x, in much better agreement with the observations, strongly suggests an underestimation of local/regional sources and an influence from both Utqiaġvik and NSA oilfield emissions. While low BC on 26 January is not resolved by these sensitivity tests (possibly due to a change in simulated air masses arriving at the site), these results could point to an underestimation in these Alaskan emissions in the ECLIPSE v6b inventory. However, the extent to which this is the case requires further investigation. *Ioannidis et al. (2023)* also noted that underestimation of nss-SO_4^{2-} in WRF-Chem simulations

This article is protected by copyright. All rights reserved.

Author Manuscript

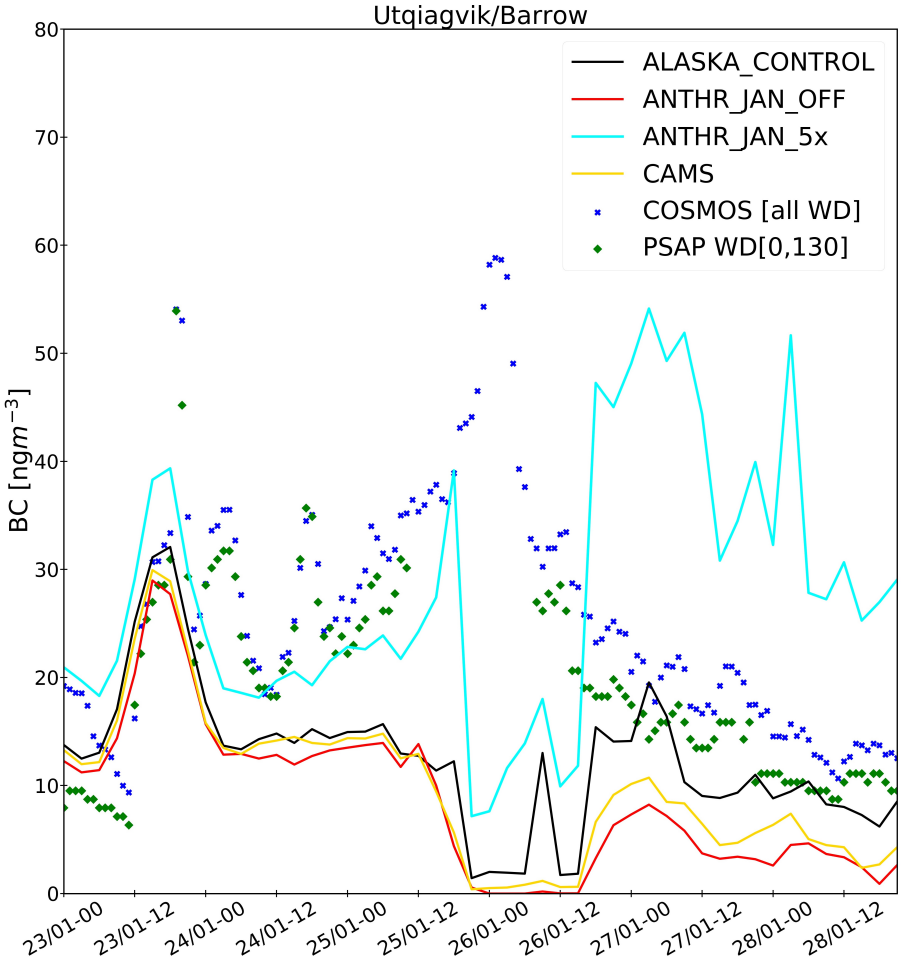


Figure 11. Modeled compared to observed sub-micron BC at Utqiaġvik/Barrow, in ng m^{-3}, from 23 to 28 January 2014. Solid lines show model results at 20 km from the runs ALASKA_CONTROL (black), CAMS_ANTHR (gold), ANTHR_OFF (red), and ANTHR_5x (turquoise). Observations are blue crosses (COSMOS) and green diamonds (PSAP). Model and observations are sub-micron BC in UTC.

of these winter 2014 campaigns could be due to underestimation of Alaskan anthropogenic emissions. Results using the CAMS emissions are lower than ALASKA_CONTROL indicating that CAMS underestimates regional Alaskan emissions more than ECLIPSE. These findings imply that it is important to take local and regional anthropogenic BC emissions into account when evaluating modeled BC against observations. It also appears that wind direction criteria applied to the PSAP data may not be filtering out all local emission influences. This is to be expected since filtering based solely on wind direction will not capture re-circulation events*(Sheridan et al., 2016)*.

Model results for the campaign period at the end of February 2014 were analyzed in detail in *Ioannidis et al. (2023)* for SSA and inorganic aerosols. The results showed higher observed nss-SO_4^{2-} during easterly or south-easterly winds that *Kirpes et al. (2018)* attributed to Prudhoe Bay origins. There are also local (town) influences as shown by the observations in Fig. 3. Fig. D1 shows the time series of observed BC against ALASKA_CONTROL, ANTHR_FEB_OFF and ANTHR_FEB_5x simulations during February 2014. The model captures better the observed BC variability (25 to 90 ng m^{-3}) when affected by

This article is protected by copyright. All rights reserved.

Author Manuscript

air masses originating from Prudhoe Bay (e.g. between 25 to 26 February compared to 27 to 28 February). The two sensitivity runs (ANTHR_OFF and ANTHR_5x) show that regional BC influence from the NSA oil-fields is higher between 25 to 26 February, and that their influence may be underestimated on 27-28 February. Overall, during this February time period there is a strong influence, 50% on average, on BC at Utqiaġvik/Barrow, due to air masses originating from the NSA oil-fields, including Prudhoe Bay (see Fig. D1, in Appendix D).

7 Conclusions

Wintertime Arctic BC is simulated using the WRF-Chem model when observed BC concentrations are enhanced contributing to Arctic haze. It is a time of year when global and regional models still have difficulties simulating Arctic BC. In this study, the influence of wet and dry deposition on Arctic BC is examined as a possible cause of model biases in quasi-hemispheric runs at 100 km for January-February 2014. The sensitivity of modeled BC over northern Alaska to removal processes, PBL meteorology and regional anthropogenic emissions is also explored for a shorter period at the end of January 2014.

Results from the 100 km run highlight regional differences in wet and dry removal patterns, both spatially and with altitude. In both cases, there is significant removal over mid-latitude source regions where modeled fluxes are comparable to previous model studies. In the Arctic, wet deposition is particularly important in the regions influenced by the Pacific and North Atlantic storm tracks, where effects are found up to 8 km and 6 km, respectively. In contrast, dry deposition affects BC mainly below 2 km over continental source regions, including northern Russian in the Arctic. Comparison of modeled BC with observations at Arctic surface sites shows that, while temporal variability and increasing BC in February are captured at all sites, BC concentrations are underestimated, except at Zeppelin, where the model performs well. Such negative biases are consistent with previous studies. Model runs with wet and dry removal switched off over mid-latitude source regions, and during transport to the Arctic, provide insights into the influence of these processes on modeled BC over the Arctic, and at surface sites. The results show that modeled BC at Zeppelin is strongly impacted by wet removal during winter since this site is influenced by the North Atlantic storm track. Wet removal also affects simulated BC more than dry removal at Alert. Here, excessive wet deposition on route to the Arctic appears to be contributing to negative biases in modeled BC, although local dry deposition fluxes at Alert are higher than observation-based estimates. Utqiaġvik/Barrow, on the north coast of Alaska, is influenced by wet removal in the Pacific storm track, and also by dry removal. At this site, local modeled wet deposition fluxes are somewhat higher than observed estimates suggesting that wet removal may also be contributing to negative biases in BC concentrations at this site. However, at Tiksi, in northern Russia, modeled BC is more sensitive to dry deposition since this site is downwind of significant Russian anthropogenic sources.

These results show that Arctic wintertime BC is very sensitive to both wet and dry removal. While improved treatments of wet deposition have received some attention (e.g. *(Mori et al., 2020)*), dry deposition is largely overlooked. Interestingly, *Macdonald et al. (2017)* suggested that dry deposition may be the dominant local removal mechanism of BC at Alert, and that models may be missing mechanisms linked to dry deposition onto snow in winter. However, only a few observational estimates of wet deposition fluxes, and even more limited estimates of dry deposition fluxes, are available to evaluate modeled fluxes at Arctic sites *(Whaley et al., 2022)*. Measurements of dry and wet removal are needed in the Arctic, and over source regions, as well as Lagrangian-style measurements in the free troposphere in order to better constrain wet removal, in particular, during transport of air masses into the Arctic during winter.

This article is protected by copyright. All rights reserved.

Author Manuscript

The effects of local and regional scale processes on modeled BC are also investigated over northern Alaska in regional runs coinciding with the measurement campaign described by *Kirpes et al. (2018)* in January 2014. A series of sensitivity tests provide insights into the model behavior compared to BC observed at Utqiaġvik/Barrow, and issues related to the measurements. The short model run at 20 km captures BC better than the large-scale run at 100 km. While this is not a strict evaluation of the impact of horizontal resolution, it illustrates that model results are improved due, in part, to better resolution of the anthropogenic emissions at 20 km. Comparison of wet and dry deposition fluxes at Utqiaġvik/Barrow also suggests that changes in the simulation of removal processes at 20 km contribute to improved modeled BC on some days. For example, dry removal is stronger in closer proximity to the main emission regions associated with the NSA oil-fields, including Prudhoe Bay, in northern Alaska, and the Fairbanks urban area in the Alaskan Interior, further south. Modeled surface BC over Alaska is also sensitive to PBL meteorology since this affects vertical exchange, stability and cloud formation, and thus wet and dry removal. This is particularly important in Arctic winter environments where very stable boundary layers are difficult for models to capture *(Steeneveld, 2014; Hong & Jiang, 2024)*. Low simulated precipitation over Alaska, coupled with underestimated local wet deposition fluxes at 20 km, suggests wet removal may be too low in this region.

The influence of local and regional anthropogenic emissions on observed BC at

Utqiaġvik/Barrow are also investigated. Based on the short periods examined, the results show that, on average, 30% of BC at Utqiaġvik/Barrow originates from Alaskan anthropogenic emissions during the January campaign, and more than 50%, on average, during the campaign at the end of February 2014. This site is especially influenced by NSA, including Prudhoe Bay, oil-field emissions when the winds are easterly. There is also an influence from local village of Utqiaġvik emissions as seen in COSMOS BC data which does not filter out these effects. Examination of PSAP EBC data also suggests an influence from these local emissions that may not be completely filtered out. These findings suggest that, in addition to wind direction, it may be necessary to apply more sophisticated filters to Utqiaġvik/Barrow BC observations, such as tracer markers (e.g. carbon monoxide), in order to better distinguish between air masses influenced by local/regional or remote sources. Results from the sensitivity runs also indicate that NSA oil-field and local Utqiaġvik anthropogenic BC emissions may be underestimated in ECLIPSE v6b (and CAMS). Based on this case study, the contribution of local and regional emissions to observed BC at Utqiaġvik/Barrow could be even higher, and merits further investigation.

Overall, the results presented in this study show that wintertime Arctic BC is sensitive to both wet and dry removal, not only over mid-latitude source regions, but also during transport, and within the Arctic with significant spatial variability, depending on location. Modeled Arctic BC is also significantly influenced by local and regional emissions over northern Alaska. This could also be the case at other Arctic sites since negative model biases in BC concentrations are linked to underestimation of episodic BC enhancements in the observations that could be due to local or regional Arctic emissions. These findings suggest that improved emission inventories are needed at higher resolution with more detailed representation of local sources over the Arctic. Improved representation of emissions and removal processes are needed to improve simulations of Arctic BC, and quantification of BC impacts on climate warming and regional air pollution, especially since new Arctic development under a warming climate may lead to increases in Arctic emissions *(Schmale et al., 2018)*.

This article is protected by copyright. All rights reserved.

Author Manuscript

8 Data Availability Statement

NCEP FNL reanalysis data obtained from https://rda.ucar.edu/datasets/ds083.2/. ECLIPSE v6b emissions are described in *Arctic Monitoring and Assessment Programme (AMAP) (2021)* and available via

https://iiasa.ac.at/models-tools-data/global-emission-fields-of-air-pollutants-and-ghgs (last access: 2020; *International Institute for Applied Systems Analysis (IIASA) (2021)*), while CAMS emissions are available from https://eccad.aeris-data.fr. Hourly average aethalometer observations for Zeppelin are available from EBAS (https://ebas.nilu.no). The data used in this study for Alert were provided by Sangeeta Sharma. Elisabeth Andrews provided Tiksi aethalometer data and Utqiaġvik/Barrow PSAP data. Sho Ohata provided COSMOS BC data from Utqiaġvik/Barrow. Meteorological data used in this study at Utqiaġvik/Barrow are from the National Oceanic and Atmospheric Administration/Earth System Research Laboratory/Global Monitoring Division (NOAA/ESRL/GMD) Baseline Observatories

(https://www1.ncdc.noaa.gov/pub/data/igra/ (last access: 2020 *Durre et al. (2018)*). Radiosonde data (every 12h) are derived from the Integrated Global Radiosonde Archive version 2 (IGRA 2) *(Durre et al., 2018)*). All observations used in this study are available in a public repository: https://doi.org/10.5281/zenodo.13882816

This article is protected by copyright. All rights reserved.

Author Manuscript

Appendix A

Table A1. Statistical metrics used to evaluate the model, where $x_{mod,i}$ and $x_{obs,i}$ are modeled and observed values.

Statistical metrics	Definition/units	Equation
Bias	ng m^{-3}	Model average minus observations average
RMSE	Root Mean Square Error in ng m^{-3}	$RMSE = \sqrt{\frac{1}{n}\sum_{i=1}^{n}(x_{mod,i} - x_{obs,i})^2}$
NME	Normalized Mean Error in %	$NME = \frac{\sum_{i=1}^{n}\lvert x_{mod,i} - x_{obs,i}\rvert}{\sum_{i=1}^{n} x_{obs,i}} * 100\%$
NMB	Normalized Mean Bias in %	$NMB = \frac{\sum_{i=1}^{n}(x_{mod,i} - x_{obs,i})}{\sum_{i=1}^{n} x_{obs,i}} * 100\%$

Appendix B

Table B1. Average percentage (%) BC change in January - February 2014, due to wet deposition switched off, at 2, 4, 6 and 8 km and at four remote Arctic sites. BC change is calculated as in Table 4. See main text for details.

	2 km	4 km	6 km	8 km
Utqiaġvik/Barrow	353	353	325	252
Alert	592	449	399	275
Tiksi	456	344	304	230
Zeppelin	769	623	499	367

Table B2. Absolute changes in BC, in ng m^{-3}, averaged over January-February 2014, due to wet deposition OFF at 2, 4, 6 and 8 km, at four remote Arctic sites. Absolute changes are calculated as the average differences between the WET_DEP_OFF and CONTROL simulations.

	2 km	4 km	6 km	8 km
Utqiaġvik/Barrow	138	171	165	151
Alert	113	100	80	52
Tiksi	136	170	185	148
Zeppelin	138	154	163	156

This article is protected by copyright. All rights reserved.

Author Manuscript

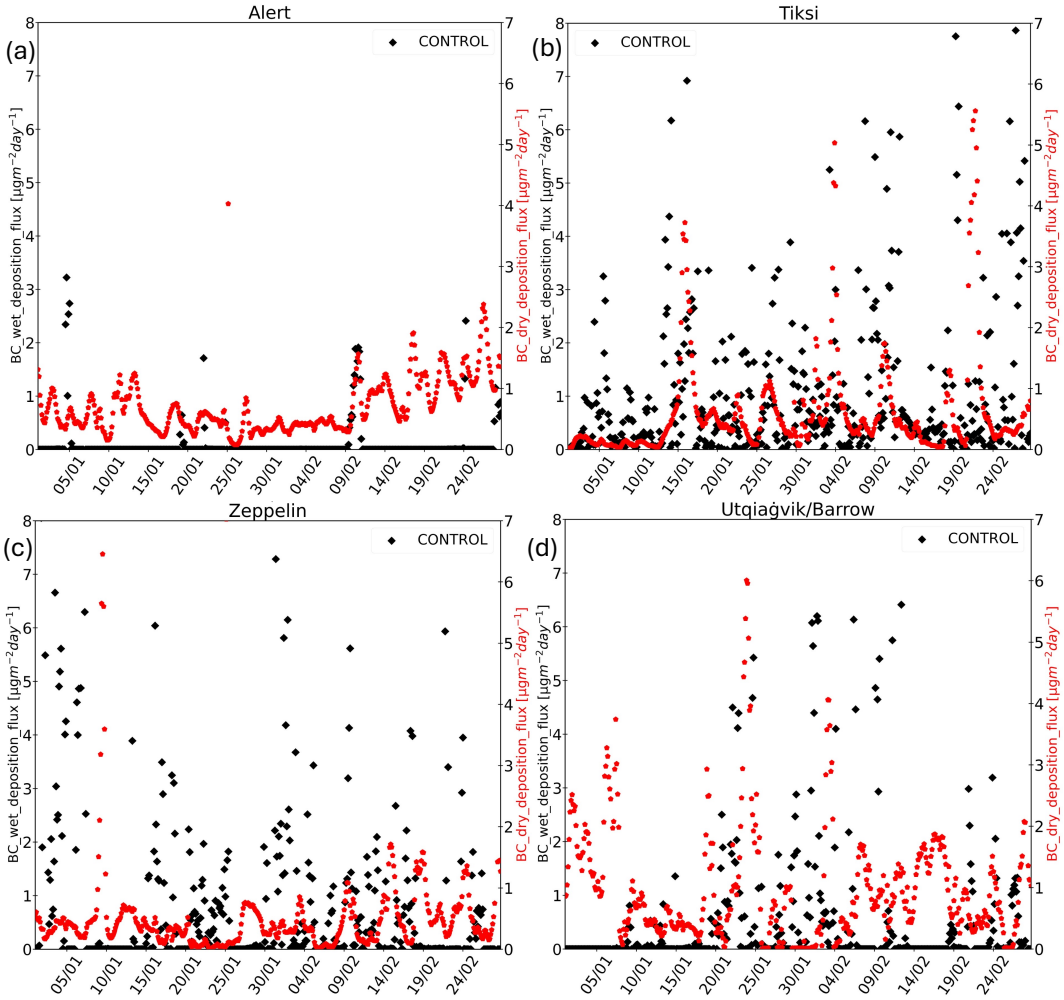


Figure B1. Timeseries of modeled wet (black) and dry (red) deposition fluxes in g m^{-2} day^{-1} for BC at (a) Alert, (b) Tiksi, (c) Zeppelin and (d) Utqiaġvik/Barrow at 100 km, during January and February 2014, using the model results from the CONTROL simulation. Results are 3-hourly.

Appendix C

ALASKA_CONTROL run with the YSU PBL scheme, and a run using the MYJ PBL scheme (METEO), are evaluated against in-situ observations and radiosondes at Barrow/Utqiaġvik, Alaska.

MYJ is a local 1.5 order scheme, with the Eta-similarity surface-layer scheme *(Tastula & Vihma, 2011)*. Briefly, MYJ determines spatially varying viscosities based on turbulent kinetic energy, local gradients, and a diagnosed length scale. *Sterk et al. (2015, 2016)* used MYJ for WRF simulations over snow-covered surfaces, coupled with the NOAH land surface model (LSM), and reported that the model was better able to capture observed winds during late winter and spring.

Figure C1 shows the time series of observed hourly 2 m and 10 m temperatures, 10 m winds speeds and wind direction compared to results from ALASKA_CONTROL and METEO at 20 km between 23 and 28 January 2014. METEO is slightly warmer than ALASKA_CONTROL, and sometimes better at capturing observed temperature variability. On the other hand, METEO is more windy and there are larger discrepancies

This article is protected by copyright. All rights reserved.

Author Manuscript

compared to observed wind directions. Overall ALASKA_CONTROL performs better than METEO, based on lower biases and RMSEs for 2 m temperature and 10 m winds (Table C1). There are also differences between the two simulations and radiosonde observations at Utqiaġvik/Barrow (Figure C2). Both simulations are more windy compared to the observations in the first 150 m, while between 200 m and 400 m METEO performs slightly better than ALASKA_CONTROL with respect to the observations. Both simulations show discrepancies regarding relative humidity and wind direction at higher altitudes. Discrepancies in wind direction and wind speeds at higher altitudes between model runs and observations could affect BC locally.

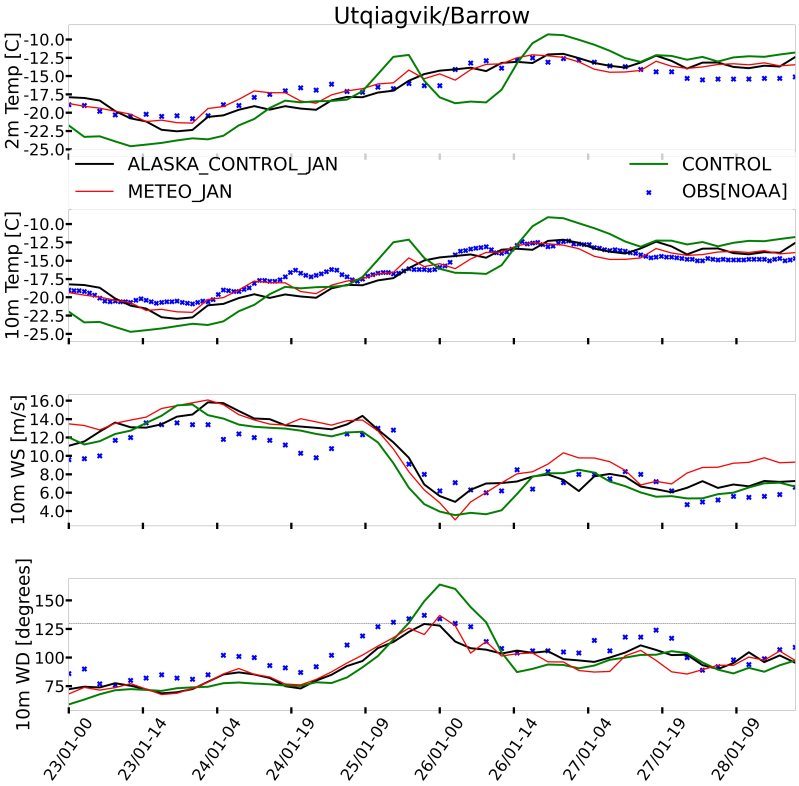


Figure C1. Time series of 2 m and 10 m temperature, 10m wind speed and wind direction during 23-28 January 2014, at Utqiaġvik/Barrow. The black line shows the model results for ALASKA_CONTROL simulation, the red line for METEO at 20 km and the green line shows the CONTROL at 100 km. Observations, in blue, are hourly data, while model output is every 3h. Both are in UTC.

Precipitation data from Applied Climate Information System, NOAA Regional Climate Centers is used to validate METEO and ALASKA_CONTROL results at 3 sites in northern Alaska. At Nome, a coastal site, on the west of Alaska, and Fairbanks, precipitation and snowfall were observed on 24 January, while a precipitation (snow) event was observed at Utqiaġvik/Barrow on 25 January (in UTC). On average over the January campaign period, both simulations underestimate observed precipitation and snowfall amounts regionally, with differences ranging from 2.5 up to 20 mm at these Alaskan sites (not shown here). Both simulations also underestimate the precipitation event (0.75 mm observed compared to 0.45 mm in ALASKA_CONTROL) at Utqiaġvik airport on

This article is protected by copyright. All rights reserved.

Author Manuscript

Table C1. Statistical analysis between CONTROL, ALASKA_CONTROL, METEO and in-situ meteorological parameters, which derived from NOAA Baseline Observatories, during January simulation. Bias is calculated as the difference between model simulation and observations.

	CONTROL		ALASKA_CONTROL		METEO	
	Bias	RMSE	Bias	RMSE	Bias	RMSE
2m Temperature	-0.4	3	0.05	1.45	0.31	1.1
10m Temperature	-0.2	2.8	-0.26	1.40	-0.25	1.01
10m Wind speed	0.1	1.8	0.86	1.63	1.6	2.46
10m Wind direction	-10	17	-9.45	11.91	-10.70	13.32

862 25 January. METEO performs only slightly better than ALASKA_CONTROL with 0.1
863 mm more precipitation.

This article is protected by copyright. All rights reserved.

Author Manuscript

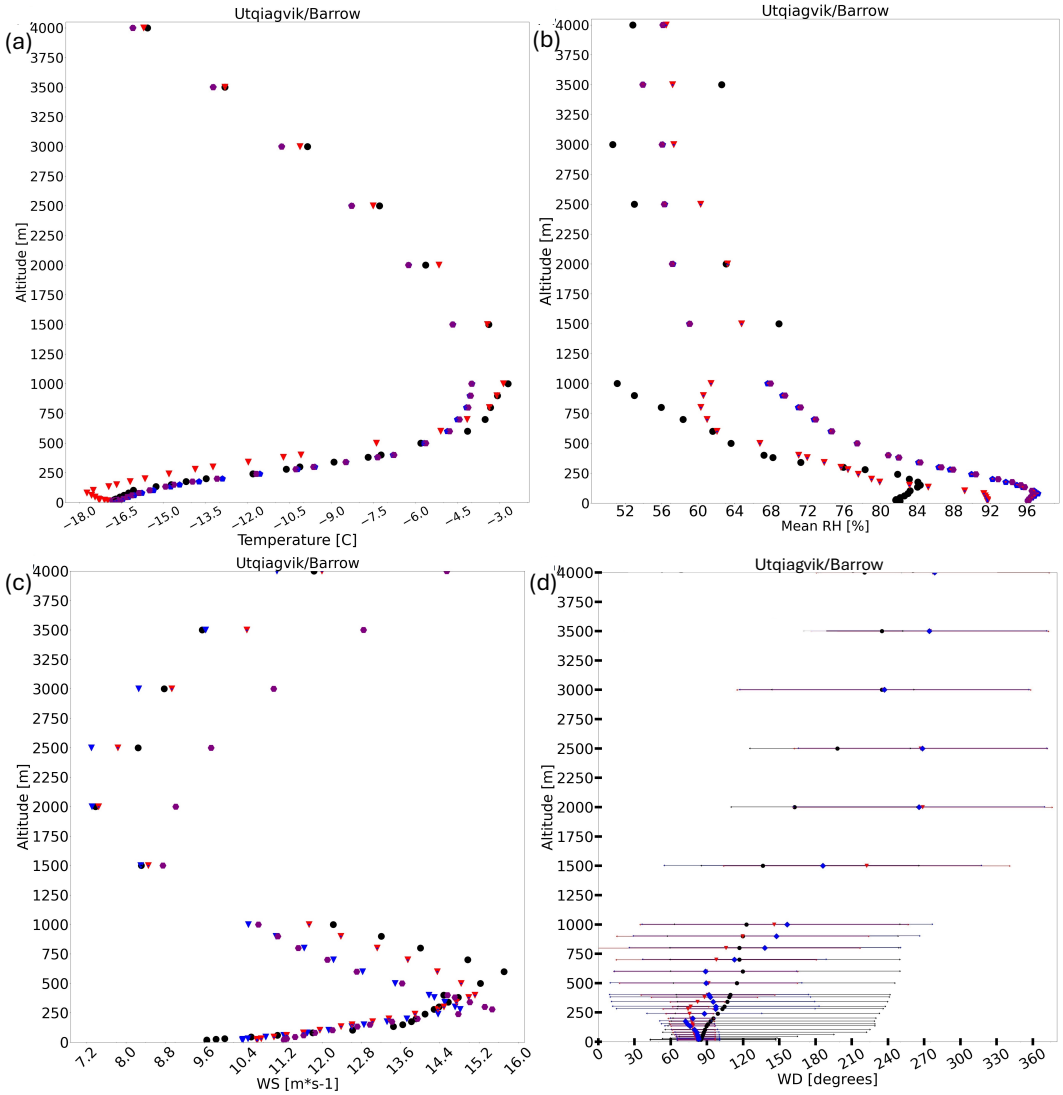


Figure C2. Comparison of model results with average radiosonde profiles for (a) temperature, (b) relative humidity (RH), (c) wind speed and (d) wind direction at Utqiaġvik/Barrow, Alaska over 23-28 January 2014. Model results are averages of 3-hourly output from ALASKA_CONTROL (red triangles) and METEO (blue triangles). for the METEO simulations. Observations are shown by black circles (averages of 12-hourly data). The corresponding lines show standard deviations.

Appendix D

This article is protected by copyright. All rights reserved.

Author Manuscript

Table C2. Statistical metrics, calculated as in Table 3, Section 4.2, between three different runs, for Utqiaġvik/Barrow, averaged over 23-28 January 2014. Numbers on the left are for model comparisons with COSMOS BC data while numbers on the right are comparisons with PSAP data. Model and observed daily (24h) averages are used to calculate the statistical metrics.

Statistic metrics/Sites	CONTROL(100 km)	ALASKA_CONTROL (20 km)	METEO (20 km)
RMSE (ng m^{-3})	20/12.6	16/9.1	17/10
Bias (ng m^{-3})	-16/-7.3	-13/-6.6	-14/-7.4
Median model (ng m^{-3})	6.2/11.5	12/12	11/10.6
Median observations (COSMOS/PSAP) (ng m^{-3})		25.0/20	
NME	61%/60%	51%/41%	53%/45%
NMB	-61%/-37%	-51%/-34%	-53%/-39%

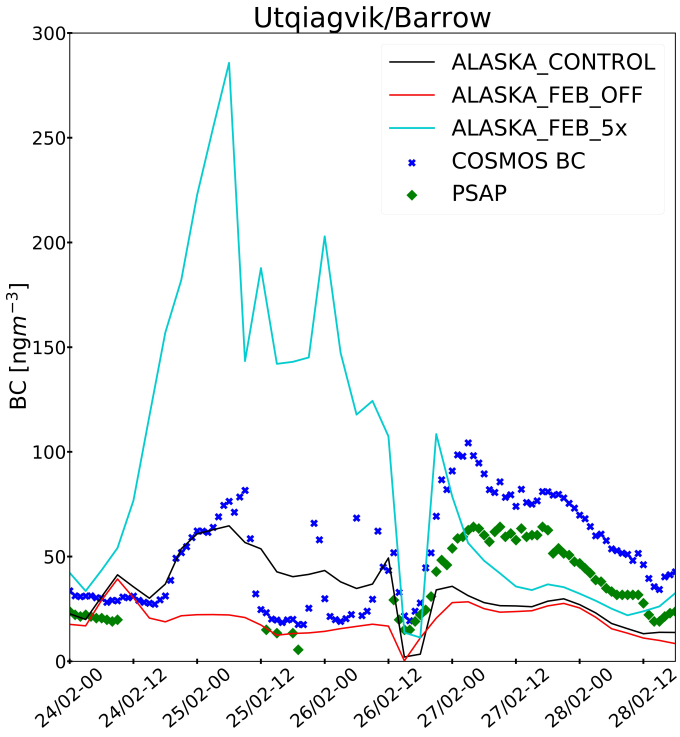


Figure D1. Modeled compared to observed sub-micron BC at Utqiaġvik/Barrow, in ng m^{-3}, from 24 to 28 February 2014. Solid lines show model results at 20 km from the runs ALASKA CONTROL (black), ANTHR OFF (red), and ANTHR 5x (turquoise). Observations are blue crosses (COSMOS) and green diamonds (PSAP). Model and observations are sub-micron BC in UTC. See Section 6.3 for further details and discussion of this figure.

This article is protected by copyright. All rights reserved.

Author Manuscript

Acknowledgments

E.I., K.S.L., J-C.R., L.M., and T.O benefited from IDRIS HPC resources (GENCI allocations A009017141, A011017141, A013017141), and the IPSL mesoscale computing center (CICLAD: Calcul Intensif pour le Climat, l'Atmosphère et la Dynamique) for the WRF-Chem model simulations. We also acknowledge the use of MOZART-4 global model output available at

`http://www.acom.ucar.edu/wrf-chem/mozart.shtml` (last access: 2019), and the WRF-Chem preprocessor tool mozbc provided by the Atmospheric Chemistry Observations and Modeling Lab (ACOM) of NCAR. E.I., K.S.L. J.-C.R., and T.O acknowledge support from the French Agence National de Recherche (ANR) CASPA (Climate-relevant Aerosol Sources and Processes in the Arctic) project (grant no. ANR-21-CE01-0017).

The following European Commission 7$^{\text{th}}$ Framework funded projects are acknowledged for the emission data, (i) ECLIPSE (Evaluating the Climate and Air Quality Impacts of Short-Lived Pollutants) Project no. 282688, (ii) PEGASOS (Pan-European Gas-Aerosols-Climate Interaction Study) Project no. 265148, and (iii) Assessment of hemispheric air pollution on EU air policy' contract no. 07.0307/2011/605671/SER/C3. K.A.P. acknowledges funding from the US National Science Foundation (OPP-1724585). E.A.'s contribution was supported in part by the Atmospheric Radiation Measurement (ARM) user facility, a US Department of Energy (DOE) Office of Science user facility managed by the Biological and Environmental Research program. This is PMEL contribution number 5420. Y.K. acknowledges support from MEXT/JSPS KAKENHI Grant no. 20H00638), MEXT Arctic Challenge for Sustainability phase II (ArCS II; JPMXD1420318865) project, and the Environment Research and Technology Development Fund 2-2301 (JPMEERF20232001) of the Restoration and Conservation Agency of Japan. For black carbon data at Alert, the authors would like to thank Canadian Forces Services for maintaining the Alert base, as well as technicians and operators for maintaining the instruments in Canadian Aerosol Baseline Measurements Network.

References

Amann, M., Bertok, I., Borken-Kleefeld, J., Cofala, J., Heyes, C., Höglund-Isaksson, L., ... others (2011). Cost-effective control of air quality and greenhouse gases in europe: Modeling and policy applications. *Environmental Modelling & Software*, *26*(12), 1489–1501.

AMAP. (2015). Amap assessment 2015: Black carbon and ozone as arctic climate forcers.

Arctic Monitoring and Assessment Programme (AMAP). (2021). *AMAP Assessment 2021: Impacts of Short-lived Climate Forcers on Arctic Climate, Air Quality, and Human Health.* Tromsø, Norway: Arctic Monitoring and Assessment Programme (AMAP).

Asmi, E., Kondratyev, V., Brus, D., Laurila, T., Lihavainen, H., Backman, J., ... others (2016). Aerosol size distribution seasonal characteristics measured in tiksi, russian arctic. *Atmospheric Chemistry and Physics*, *16*(3), 1271–1287.

Backman, J., Schmeisser, L., & Asmi, E. (2021). Asian emissions explain much of the arctic black carbon events. *Geophysical Research Letters*, *48*(5), e2020GL091913. Retrieved from `https://agupubs.onlinelibrary.wiley.com/doi/abs/10.1029/2020GL091913` (e2020GL091913 2020GL091913) doi: https://doi.org/10.1029/2020GL091913

Backman, J., Schmeisser, L., Virkkula, A., Ogren, J. A., Asmi, E., Starkweather, S., ... others (2017). On aethalometer measurement uncertainties and an instrument correction factor for the arctic. *Atmospheric Measurement Techniques*, *10*(12), 5039–5062.

Barrett, T., Robinson, E., Usenko, S., & Sheesley, R. (2015). Source contributions

This article is protected by copyright. All rights reserved.

Author Manuscript

to wintertime elemental and organic carbon in the western arctic based on radiocarbon and tracer apportionment. *Environmental science & technology*, *49*(19), 11631–11639.

Barrie, L., Hoff, R., & Daggupaty, S. (1981). The influence of mid-latitudinal pollution sources on haze in the canadian arctic. *Atmospheric Environment (1967)*, *15*(8), 1407–1419.

Barrie, L., Staebler, R., Toom, D., Georgi, B., Den Hartog, G., Landsberger, S., & Wu, D. (1994). Arctic aerosol size-segregated chemical observations in relation to ozone depletion during polar sunrise experiment 1992. *Journal of Geophysical Research: Atmospheres*, *99*(D12), 25439–25451.

Bei, N., Li, G., & Molina, L. (2012). Uncertainties in soa simulations due to meteorological uncertainties in mexico city during milagro-2006 field campaign. *Atmospheric Chemistry and Physics*, *12*(23), 11295–11308.

Berg, L. K., Shrivastava, M., Easter, R. C., Fast, J. D., Chapman, E. G., Liu, Y., & Ferrare, R. (2015). A new wrf-chem treatment for studying regional-scale impacts of cloud processes on aerosol and trace gases in parameterized cumuli. *Geoscientific Model Development*, *8*(2), 409–429.

Binkowski, F. S., & Shankar, U. (1995). The regional particulate matter model: 1. model description and preliminary results. *Journal of Geophysical Research: Atmospheres*, *100*(D12), 26191–26209.

Bond, T. C., Anderson, T. L., & Campbell, D. (1999). Calibration and intercomparison of filter-based measurements of visible light absorption by aerosols. *Aerosol Science & Technology*, *30*(6), 582–600.

Bourgeois, Q., & Bey, I. (2011). Pollution transport efficiency toward the arctic: Sensitivity to aerosol scavenging and source regions. *Journal of Geophysical Research: Atmospheres*, *116*(D8).

Brümmer, B., & Thiemann, S. (2002). The atmospheric boundary layer in an arctic wintertime on-ice air flow. *Boundary-layer meteorology*, *104*, 53–72.

Carter, W. P. (2000). Documentation of the saprc-99 chemical mechanism for voc reactivity assessment. *Contract*, *92*(329), 95–308.

Chapman, E. G., Gustafson Jr, W., Easter, R. C., Barnard, J. C., Ghan, S. J., Pekour, M. S., & Fast, J. D. (2009). Coupling aerosol-cloud-radiative processes in the wrf-chem model: Investigating the radiative impact of elevated point sources. *Atmospheric Chemistry and Physics*, *9*(3), 945–964.

Chen, X., Kang, S., & Yang, J. (2020). Investigation of distribution, transportation, and impact factors of atmospheric black carbon in the arctic region based on a regional climate-chemistry model. *Environmental Pollution*, *257*, 113127.

Crippa, M., Guizzardi, D., Muntean, M., Schaaf, E., & Oreggioni, G. (2019). *Edgar v5. 0 global air pollutant emissions, european commission, joint research centre (jrc)[data set].*

Durre, I., Yin, X., Vose, R. S., Applequist, S., & Arnfield, J. (2018). Enhancing the data coverage in the integrated global radiosonde archive. *Journal of Atmospheric and Oceanic Technology*, *35*(9), 1753–1770.

Easter, R. C., Ghan, S. J., Zhang, Y., Saylor, R. D., Chapman, E. G., Laulainen, N. S., ... Zaveri, R. A. (2004). Mirage: Model description and evaluation of aerosols and trace gases. *Journal of Geophysical Research: Atmospheres*, *109*(D20).

Eckhardt, S., Quennehen, B., Oliviè, D. J. L., Berntsen, T. K., Cherian, R., Christensen, J., ... others (2015). Current model capabilities for simulating black carbon and sulfate concentrations in the arctic atmosphere: a multi-model evaluation using a comprehensive measurement data set. *Atmospheric Chemistry and Physics*, *15*(16), 9413–9433.

Eleftheriadis, K., Vratolis, S., & Nyeki, S. (2009). Aerosol black carbon in the european arctic: Measurements at zeppelin station, ny-Ålesund, svalbard from 1998–2007. *Geophysical Research Letters*, *36*(2). doi: https://doi.org/10.1029/

This article is protected by copyright. All rights reserved.

Author Manuscript

2008GL035741

Emmons, L. K., Walters, S., Hess, P. G., Lamarque, J.-F., Pfister, G. G., Fillmore, D., ... others (2010). Description and evaluation of the model for ozone and related chemical tracers, version 4 (mozart-4). *Geoscientific Model Development*, *3*(1), 43–67.

Flanner, M. G. (2013). Arctic climate sensitivity to local black carbon. *Journal of Geophysical Research: Atmospheres*, *118*(4), 1840–1851.

Freud, E., Krejci, R., Tunved, P., Leaitch, R., Nguyen, Q. T., Massling, A., ... Barrie, L. (2017). Pan-arctic aerosol number size distributions: seasonality and transport patterns. *Atmospheric Chemistry and Physics*, *17*(13), 8101–8128.

Gilardoni, S., Heslin-Rees, D., Mazzola, M., Vitale, V., Sprenger, M., & Krejci, R. (2023). Drivers controlling black carbon temporal variability in the lower troposphere of the european arctic. *Atmospheric Chemistry and Physics*, *23*(24), 15589–15607.

Grell, G. A., Peckham, S. E., Schmitz, R., McKeen, S. A., Frost, G., Skamarock, W. C., & Eder, B. (2005). Fully coupled "online" chemistry within the wrf model. *Atmospheric Environment*, *39*(37), 6957–6975.

Guenther, A., Jiang, X., Heald, C. L., Sakulyanontvittaya, T., Duhl, T., Emmons, L., & Wang, X. (2012). The model of emissions of gases and aerosols from nature version 2.1 (megan2. 1): an extended and updated framework for modeling biogenic emissions. *Geoscientific Model Development*, *5*(6), 1471–1492.

Heslin-Rees, D., Tunved, P., Ström, J., Cremer, R., Zieger, P., Riipinen, I., ... Krejci, R. (2024). Increase in precipitation scavenging contributes to long-term reductions of light-absorbing aerosol in the arctic. *Atmospheric Chemistry and Physics*, *24*(4), 2059–2075.

Hodnebrog, Ø., Marelle, L., Alterskjær, K., Wood, R. R., Ludwig, R., Fischer, E. M., ... Myhre, G. (2019). Intensification of summer precipitation with shorter time-scales in europe. *Environmental Research Letters*, *14*(12), 124050.

Höglund-Isaksson, L., Gómez-Sanabria, A., Klimont, Z., Rafaj, P., & Schöpp, W. (2020). Technical potentials and costs for reducing global anthropogenic methane emissions in the 2050 timeframe–results from the gains model. *Environmental Research Communications*, *2*(2), 025004.

Hong, X., & Jiang, Q. (2024). Impact of land surface snow processes on the arctic stable boundary layer. *Journal of Hydrometeorology*, *25*(3), 479–494.

Ikeda, K., Tanimoto, H., Sugita, T., Akiyoshi, H., Kanaya, Y., Zhu, C., & Taketani, F. (2017). Tagged tracer simulations of black carbon in the arctic: transport, source contributions, and budget. *Atmospheric Chemistry and Physics*, *17*(17), 10515–10533. Retrieved from `https://acp.copernicus.org/articles/17/10515/2017/` doi: 10.5194/acp-17-10515-2017

International Institute for Applied Systems Analysis (IIASA). (2021). *Eclipse v6b global emission fields.* Retrieved from `https://previous.iiasa.ac.at/web/home/research/researchPrograms/air/ECLIPSEv6b.html` (Last accessed: 2020)

Ioannidis, E., Law, K. S., Raut, J.-C., Marelle, L., Onishi, T., Kirpes, R. M., ... Pratt, K. A. (2023). Modelling wintertime sea-spray aerosols under arctic haze conditions. *Atmospheric Chemistry and Physics*, *23*(10), 5641–5678. Retrieved from `https://acp.copernicus.org/articles/23/5641/2023/` doi: 10.5194/acp-23-5641-2023

IPCC. (2021). Ipcc, 2021: Summary for policymakers. in: Climate change 2021: The physical science basis. contribution of working group i to the sixth assessment report of the intergovernmental panel on climate change [masson-delmotte, v., p. zhai, a. pirani, s.l. connors, c. péan, s. berger, n. caud, y. chen, l. goldfarb, m.i. gomis, m. huang, k. leitzell, e. lonnoy, j.b.r. matthews, t.k. maycock, t. waterfield, o. yelekçi, r. yu, and b. zhou (eds.)]. , pp. 332. doi:

This article is protected by copyright. All rights reserved.

Author Manuscript

doi:10.1017/9781009157896.001.

Jacobi, H.-W., Obleitner, F., Da Costa, S., Ginot, P., Eleftheriadis, K., Aas, W., & Zanatta, M. (2019). Deposition of ionic species and black carbon to the arctic snowpack: combining snow pit observations with modeling. *Atmospheric Chemistry and Physics*, *19*(15), 10361–10377.

Jiao, C., Flanner, M. G., Balkanski, Y., Bauer, S. E., Bellouin, N., Berntsen, T. K., ... Zhang, K. (2014). An aerocom assessment of black carbon in arctic snow and sea ice. *Atmospheric Chemistry and Physics*, *14*(5), 2399–2417. Retrieved from `https://acp.copernicus.org/articles/14/2399/2014/` doi: 10.5194/acp-14-2399-2014

Kirpes, R. M., Bonanno, D., May, N. W., Fraund, M., Barget, A. J., Moffet, R. C., ... Pratt, K. A. (2019). Wintertime arctic sea spray aerosol composition controlled by sea ice lead microbiology. *ACS Central Science*, *5*(11), 1760-1767. Retrieved from `https://doi.org/10.1021/acscentsci.9b00541` doi: 10.1021/acscentsci.9b00541

Kirpes, R. M., Bondy, A. L., Bonanno, D., Moffet, R. C., Wang, B., Laskin, A., ... Pratt, K. A. (2018). Secondary sulfate is internally mixed with sea spray aerosol and organic aerosol in the winter arctic. *Atmospheric Chemistry and Physics*, *18*(6), 3937–3949. Retrieved from `https://acp.copernicus.org/articles/18/3937/2018/` doi: 10.5194/acp-18-3937-2018

Klimont, Z., Kupiainen, K., Heyes, C., Purohit, P., Cofala, J., Rafaj, P., ... Schöpp, W. (2017). Global anthropogenic emissions of particulate matter including black carbon. *Atmospheric Chemistry and Physics*, *17*(14), 8681–8723.

Kolesar, K. R., Cellini, J., Peterson, P. K., Jefferson, A., Tuch, T., Birmili, W., ... Pratt, K. A. (2017). Effect of prudhoe bay emissions on atmospheric aerosol growth events observed in utqiaġvik (barrow), alaska. *Atmospheric Environment*, *152*, 146-155. Retrieved from `https://www.sciencedirect.com/science/article/pii/S1352231016309785` doi: https://doi.org/10.1016/j.atmosenv.2016.12.019

Kondo, Y., Sahu, L., Kuwata, M., Miyazaki, Y., Takegawa, N., Moteki, N., ... others (2009). Stabilization of the mass absorption cross section of black carbon for filter-based absorption photometry by the use of a heated inlet. *Aerosol Science and Technology*, *43*(8), 741–756.

Kondo, Y., Sahu, L., Moteki, N., Khan, F., Takegawa, N., Liu, X., ... Miyakawa, T. (2011). Consistency and traceability of black carbon measurements made by laser-induced incandescence, thermal-optical transmittance, and filter-based photo-absorption techniques. *Aerosol Science and Technology*, *45*(2), 295–312.

Leaitch, W. R., Russell, L. M., Liu, J., Kolonjari, F., Toom, D., Huang, L., ... Zhang, W. (2018a). Organic functional groups in the submicron aerosol at 82.5° n, 62.5° w from 2012 to 2014. *Atmospheric Chemistry and Physics*, *18*(5), 3269–3287. Retrieved from `https://acp.copernicus.org/articles/18/3269/2018/` doi: 10.5194/acp-18-3269-2018

Leaitch, W. R., Russell, L. M., Liu, J., Kolonjari, F., Toom, D., Huang, L., ... Zhang, W. (2018b). Organic functional groups in the submicron aerosol at 82.5 n, 62.5 w from 2012 to 2014. *Atmospheric Chemistry and Physics*, *18*(5), 3269–3287.

Liu, J., Fan, S., Horowitz, L. W., & Levy, H. (2011). Evaluation of factors controlling long-range transport of black carbon to the arctic. *Journal of Geophysical Research: Atmospheres*, *116*(D4).

Liu, M., & Matsui, H. (2021). Improved simulations of global black carbon distributions by modifying wet scavenging processes in convective and mixed-phase clouds. *Journal of Geophysical Research: Atmospheres*, *126*(3), e2020JD033890.

Luo, G., Yu, F., & Moch, J. M. (2020). Further improvement of wet process treatments in geos-chem v12. 6.0: impact on global distributions of aerosols and

This article is protected by copyright. All rights reserved.

Author Manuscript

aerosol precursors. *Geoscientific Model Development*, *13*(6), 2879–2903.

Ma, P.-L., Rasch, P. J., Wang, H., Zhang, K., Easter, R. C., Tilmes, S., ... Lamarque, J.-F. (2013). The role of circulation features on black carbon transport into the arctic in the community atmosphere model version 5 (cam5). *Journal of Geophysical Research: Atmospheres*, *118*(10), 4657–4669.

Macdonald, K. M., Sharma, S., Toom, D., Chivulescu, A., Hanna, S., Bertram, A. K., ... Abbatt, J. P. D. (2017). Observations of atmospheric chemical deposition to high arctic snow. *Atmospheric Chemistry and Physics*, *17*(9), 5775–5788. Retrieved from `https://acp.copernicus.org/articles/17/5775/2017/` doi: 10.5194/acp-17-5775-2017

Mahmood, R., von Salzen, K., Flanner, M., Sand, M., Langner, J., Wang, H., & Huang, L. (2016). Seasonality of global and arctic black carbon processes in the arctic monitoring and assessment programme models. *Journal of Geophysical Research: Atmospheres*, *121*(12), 7100–7116.

Marelle, L., Raut, J.-C., Law, K. S., Berg, L. K., Fast, J. D., Easter, R. C., ... Thomas, J. L. (2017). Improvements to the wrf-chem 3.5.1 model for quasi-hemispheric simulations of aerosols and ozone in the arctic. *Geoscientific Model Development*, *10*(10), 3661–3677. Retrieved from `https://gmd.copernicus.org/articles/10/3661/2017/` doi: 10.5194/gmd-10-3661-2017

Matsui, H., Mori, T., Ohata, S., Moteki, N., Oshima, N., Goto-Azuma, K., ... Kondo, Y. (2022). Contrasting source contributions of arctic black carbon to atmospheric concentrations, deposition flux, and atmospheric and snow radiative effects. *Atmospheric Chemistry and Physics Discussions*, 1–31.

McDuffie, E. E., Smith, S. J., O'Rourke, P., Tibrewal, K., Venkataraman, C., Marais, E. A., ... Martin, R. V. (2020). A global anthropogenic emission inventory of atmospheric pollutants from sector-and fuel-specific sources (1970–2017): an application of the community emissions data system (ceds). *Earth System Science Data*, *12*(4), 3413–3442.

Miyazaki, Y., Kondo, Y., Sahu, L. K., Imaru, J., Fukushima, N., & Kano, M. (2008). Performance of a newly designed continuous soot monitoring system (cosmos). *Journal of environmental monitoring*, *10*(10), 1195–1201.

Moffett, C. E., Mehra, M., Barrett, T. E., Gunsch, M. J., Pratt, K. A., & Sheesley, R. J. (2022). Contemporary sources dominate carbonaceous aerosol on the north slope of alaska. *Science of The Total Environment*, *831*, 154641. Retrieved from `https://www.sciencedirect.com/science/article/pii/S004896972201734X` doi: https://doi.org/10.1016/j.scitotenv.2022.154641

Moon, T. A., Druckenmiller, M. L., & Thoman, R. L. (Eds.). (2024). *Arctic report card 2024*. National Park Service. Retrieved from `https://www.nps.gov/articles/arcticreportcard2024.htm` (Available online: `https://www.nps.gov/articles/arcticreportcard2024.htm`)

Mori, T., Kondo, Y., Ohata, S., Goto-Azuma, K., Fukuda, K., Ogawa-Tsukagawa, Y., ... others (2021). Seasonal variation of wet deposition of black carbon at ny-ålesund, svalbard. *Journal of Geophysical Research: Atmospheres*, e2020JD034110.

Mori, T., Kondo, Y., Ohata, S., Zhao, Y., Sinha, P., Oshima, N., ... Koike, M. (2020). Seasonal variation of wet deposition of black carbon in arctic alaska. *Journal of Geophysical Research: Atmospheres*, *125*(16), e2019JD032240.

Morrison, T. G. T. V., H. (2009). Impact of cloud microphysics on the development of trailing stratiform precipitation in a simulated squall line: Comparison of one– and two–moment schemes. *Mon. Wea. Rev.*, *137*, 991—1007. doi: 10.1175/2008MWR2556.1

National Centers for Environmental Prediction, National Weather Service, NOAA, U.S. Department of Commerce. (2000). *Ncep fnl operational model global tropospheric analyses, continuing from july 1999.* Boulder CO: Research Data Archive at the National Center for Atmospheric Research, Computational and

This article is protected by copyright. All rights reserved.

Author Manuscript

Information Systems Laboratory. Retrieved from https://doi.org/10.5065/D6M043C6

Ogren, J. A. (2010). Comment on "calibration and intercomparison of filter-based measurements of visible light absorption by aerosols". *Aerosol Science and Technology*, *44*(8), 589–591.

Ohata, S., Kondo, Y., Moteki, N., Mori, T., Yoshida, A., Sinha, P. R., & Koike, M. (2019). Accuracy of black carbon measurements by a filter-based absorption photometer with a heated inlet. *Aerosol Science and Technology*, *53*(9), 1079–1091.

Ohata, S., Mori, T., Kondo, Y., Sharma, S., Hyvärinen, A., Andrews, E., ... others (2020). Estimates of mass absorption cross sections of black carbon for filter-based absorption photometers in the arctic. *Atmospheric Chemistry and Physics Discussions*, 1–38.

Popovicheva, O. B., Evangeliou, N., Kobelev, V. O., Chichaeva, M. A., Eleftheriadis, K., Gregoric, A., & Kasimov, N. S. (2022). Siberian arctic black carbon: gas flaring and wildfire impact. *Atmos. Chem. Phys*, *22*, 5983–6000.

Quinn, P. K., Bates, T. S., Baum, E., Doubleday, N., Fiore, A. M., Flanner, M., ... Warren, S. G. (2008). Short-lived pollutants in the arctic: their climate impact and possible mitigation strategies. *Atmospheric Chemistry and Physics*, *8*(6), 1723–1735. Retrieved from https://acp.copernicus.org/articles/8/1723/2008/ doi: 10.5194/acp-8-1723-2008

Quinn, P. K., Miller, T. L., Bates, T. S., Ogren, J. A., Andrews, E., & Shaw, G. E. (2002). A 3-year record of simultaneously measured aerosol chemical and optical properties at barrow, alaska. *Journal of Geophysical Research: Atmospheres*, *107*(D11), AAC 8-1-AAC 8-15. doi: https://doi.org/10.1029/2001JD001248

Rahn, K. A., & McCaffrey, R. J. (1980). On the origin and transport of the winter arctic aerosol. *Annals of the New York Academy of Sciences*, *338*(1), 486–503.

Raut, J.-C., Marelle, L., Fast, J. D., Thomas, J. L., Weinzierl, B., Law, K. S., ... others (2017). Cross-polar transport and scavenging of siberian aerosols containing black carbon during the 2012 access summer campaign. *Atmospheric Chemistry and Physics*, *17*(18), 10969–10995.

Regmi, R. P., Kitada, T., Maharjan, S., Shrestha, S., Shrestha, S., & Regmi, G. (2019). Wintertime boundary layer evolution and air pollution potential over the kathmandu valley, nepal. *Journal of Geophysical Research: Atmospheres*, *124*(8), 4299–4325.

Schmale, J., Arnold, S., Law, K. S., Thorp, T., Anenberg, S., Simpson, W., ... Pratt, K. (2018). Local arctic air pollution: A neglected but serious problem. *Earth's Future*, *6*(10), 1385–1412.

Sharma, S., Barrie, L. A., Magnusson, E., Brattström, G., Leaitch, W., Steffen, A., & Landsberger, S. (2019). A factor and trends analysis of multidecadal lower tropospheric observations of arctic aerosol composition, black carbon, ozone, and mercury at alert, canada. *Journal of Geophysical Research: Atmospheres*, *124*(24), 14133–14161.

Sharma, S., Ishizawa, M., Chan, D., Lavoué, D., Andrews, E., Eleftheriadis, K., & Maksyutov, S. (2013). 16-year simulation of arctic black carbon: Transport, source contribution, and sensitivity analysis on deposition. *Journal of Geophysical Research: Atmospheres*, *118*(2), 943–964.

Sharma, S., Leaitch, W. R., Huang, L., Veber, D., Kolonjari, F., Zhang, W., ... Ogren, J. A. (2017). An evaluation of three methods for measuring black carbon in alert, canada. *Atmospheric Chemistry and Physics*, *17*(24), 15225–15243.

Shen, Z., Ming, Y., Horowitz, L. W., Ramaswamy, V., & Lin, M. (2017). On the seasonality of arctic black carbon. *Journal of Climate*, *30*(12), 4429–4441.

Sheridan, P., Andrews, E., Schmeisser, L., Vasel, B., & Ogren, J. (2016). Aerosol

This article is protected by copyright. All rights reserved.

Author Manuscript

measurements at south pole: Climatology and impact of local contamination. *Aerosol and Air Quality Research*, *16*(3), 855–872. doi: 10.4209/aaqr.2015.05.0358

Slinn. (1982). Predictions for particle deposition to vegetative canopies. *Atmospheric Environment (1967)*, *16*(7), 1785–1794.

Slinn, & Slinn. (1980). Predictions for particle deposition on natural waters. *Atmospheric Environment (1967)*, *14*(9), 1013–1016.

Soulie, A., Granier, C., Darras, S., Zilbermann, N., Doumbia, T., Guevara, M., ... others (2023). Global anthropogenic emissions (cams-glob-ant) for the copernicus atmosphere monitoring service simulations of air quality forecasts and reanalyses. *Earth System Science Data Discussions*, *2023*, 1–45.

Steeneveld, G.-J. (2014). Current challenges in understanding and forecasting stable boundary layers over land and ice. *Frontiers in Environmental Science*, *2*, 41.

Sterk, H., Steeneveld, G., Bosveld, F., Vihma, T., Anderson, P., & Holtslag, A. (2016). Clear-sky stable boundary layers with low winds over snow-covered surfaces. part 2: Process sensitivity. *Quarterly Journal of the Royal Meteorological Society*, *142*(695), 821–835.

Sterk, H., Steeneveld, G., Vihma, T., Anderson, P., Bosveld, F., & Holtslag, A. (2015). Clear-sky stable boundary layers with low winds over snow-covered surfaces. part 1: Wrf model evaluation. *Quarterly Journal of the Royal Meteorological Society*, *141*(691), 2165–2184.

Stohl, A. (2006). Characteristics of atmospheric transport into the arctic troposphere. *Journal of Geophysical Research: Atmospheres*, *111*(D11).

Stohl, A., Klimont, Z., Eckhardt, S., Kupiainen, K., Shevchenko, V. P., Kopeikin, V. M., & Novigatsky, A. N. (2013). Black carbon in the arctic: the underestimated role of gas flaring and residential combustion emissions. *Atmospheric Chemistry and Physics*, *13*(17), 8833–8855. Retrieved from `https://acp.copernicus.org/articles/13/8833/2013/` doi: 10.5194/acp-13-8833-2013

Tastula, E.-M., & Vihma, T. (2011). Wrf model experiments on the antarctic atmosphere in winter. *Monthly Weather Review*, *139*(4), 1279–1291.

Tran, H. N., & Mölders, N. (2011). Investigations on meteorological conditions for elevated pm2. 5 in fairbanks, alaska. *Atmospheric Research*, *99*(1), 39–49.

von Salzen, K., Whaley, C. H., Anenberg, S. C., Van Dingenen, R., Klimont, Z., Flanner, M. G., ... others (2022). Clean air policies are key for successfully mitigating arctic warming. *Communications Earth & Environment*, *3*(1), 222.

Whaley, C. H., Mahmood, R., von Salzen, K., Winter, B., Eckhardt, S., Arnold, S., ... others (2022). Model evaluation of short-lived climate forcers for the arctic monitoring and assessment programme: a multi-species, multi-model study. *Atmospheric Chemistry and Physics Discussions*, 1–88.

Winiger, P., Andersson, A., Eckhardt, S., Stohl, A., Semiletov, I. P., Dudarev, O. V., ... others (2017). Siberian arctic black carbon sources constrained by model and observation. *Proceedings of the National Academy of Sciences*, *114*(7), E1054–E1061.

Winiger, P., Barrett, T., Sheesley, R., Huang, L., Sharma, S., Barrie, L. A., ... others (2019). Source apportionment of circum-arctic atmospheric black carbon from isotopes and modeling. *Science advances*, *5*(2), eaau8052.

Xu, J., Zhang, J., Liu, J., Yi, K., Xiang, S., Hu, X., ... Ban-Weiss, G. (2019). Influence of cloud microphysical processes on black carbon wet removal, global distributions, and radiative forcing. *Atmospheric Chemistry and Physics*, *19*(3), 1587–1603.

Yun, Y., Penner, J., & Popovicheva, O. (2013). The effects of hygroscopicity on ice nucleation of fossil fuel combustion aerosols in mixed-phase clouds. *Atmospheric Chemistry and Physics*, *13*(8), 4339–4348.

Zaveri, R. A., Easter, R. C., Fast, J. D., & Peters, L. K. (2008). Model for

This article is protected by copyright. All rights reserved.

simulating aerosol interactions and chemistry (mosaic). *Journal of Geophysical Research: Atmospheres*, *113*(D13). Retrieved from `https://agupubs.onlinelibrary.wiley.com/doi/abs/10.1029/2007JD008782` doi: https://doi.org/10.1029/2007JD008782

Zhu, C., Kanaya, Y., Takigawa, M., Ikeda, K., Tanimoto, H., Taketani, F., ... Pisso, I. (2020). Flexpart v10. 1 simulation of source contributions to arctic black carbon. *Atmospheric Chemistry and Physics*, *20*(3), 1641–1656.

Zieger, P., Heslin-Rees, D., Karlsson, L., Koike, M., Modini, R., & Krejci, R. (2023). Black carbon scavenging by low-level arctic clouds. *Nature communications*, *14*(1), 5488.

This article is protected by copyright. All rights reserved.

Author Manuscript